https://doi.org/10.5194/egusphere-2026-2682
Preprint. Discussion started: 3 June 2026

Potential natural vegetation as overlooked determinant of land-use change flux estimates

Adrian I. R. Jäschke[1], Wolfgang A. Obermeier[1], Clemens Schwingshackl[1], Amali A. Amali[1,2], Julia Pongratz[1], and Raphael Ganzenmüller[1]

[1]Department of Geography, Ludwig-Maximilians-Universität München, Munich, Germany
[2]GEOMAR Helmholtz Centre for Ocean Research Kiel, Kiel, Germany

Correspondence: Adrian I. R. Jäschke (Adrian.Jaeschke@lmu.de)

Abstract. The net carbon dioxide (CO_2) flux from land use and land-use change (F_{LUC}) is a major driver of anthropogenic climate change and central to mitigation strategies for achieving global emission reduction targets. Despite its importance, estimates of F_{LUC} are characterized by large uncertainties. In models quantifying F_{LUC}, the spatial distribution of potential natural vegetation (PNV) is a key component, but its influence on F_{LUC} estimates has not been systematically quantified. Here, we address this gap by combining pollen-based biome reconstructions and observation-based datasets of environmental conditions with machine learning to derive global PNV maps. Compared to existing PNV maps, our approach improves the representation of biome-specific spatial heterogeneity and provides sensitivity maps for quantifying how assumptions about potential forest and grassland distribution propagate into F_{LUC} estimates. Implementing the PNV maps as Plant Functional Types (PFTs) in the bookkeeping model BLUE, we find global cumulative F_{LUC} for the period 1850–2023 to be 16% (6–27%) higher than the default estimate. Differences at the regional scale are often even larger. Our results demonstrate that uncertainties in PNV distribution represent a substantial and previously overlooked source of uncertainty in F_{LUC} estimates, comparable in magnitude to other key sources. Accurate PNV mapping is therefore essential for robust F_{LUC} estimates, particularly at regional scales, which are required for understanding the global carbon cycle, improving F_{LUC} modeling, and informing effective climate mitigation policies.

1 Introduction

The net carbon dioxide (CO_2) flux from land use and land-use change (F_{LUC}) is a key component of the global carbon cycle and substantially contributes to global climate warming (IPCC, 2019). Since 1850, it has accounted for approximately one-third of global anthropogenic CO_2 emissions (Friedlingstein et al., 2025). F_{LUC} encompasses both CO_2 emissions from terrestrial ecosystems to the atmosphere (gross sources) and the uptake and storage of carbon from the atmosphere in vegetation and soils (gross sinks), resulting from anthropogenic land-use activities such as deforestation, agricultural expansion and abandonment, afforestation, and forest management (Pongratz et al., 2021). Limiting global warming to well-below 2 °C, aligned with the climate targets of the Paris Agreement, requires a decrease in land-use emissions and an increase in land-use removals, transforming the global net F_{LUC} from a carbon source into a sink (Harper et al., 2018; Smith et al., 2024). However, F_{LUC}

https://doi.org/10.5194/egusphere-2026-2682
Preprint. Discussion started: 3 June 2026

estimates remain one of the most uncertain components of the global carbon cycle, with a relative uncertainty of about 64% for the period 2014–2023 (Friedlingstein et al., 2025). Therefore, improvements in the accuracy of F_{LUC} quantification are crucial for understanding the global carbon cycle, projecting future climate change, informing climate policy, and supporting effective climate mitigation efforts (Smith et al., 2024).

Although major progress has been made in recent years in understanding and reducing uncertainties in F_{LUC} estimates, crucial sources of uncertainty remain unaddressed. F_{LUC} estimates are typically derived from bookkeeping models and Dynamic Global Vegetation Models (DGVMs) (Obermeier et al., 2025) and are used, for example, in the Global Carbon Budget (GCB; Friedlingstein et al., 2025) and reports of the Intergovernmental Panel on Climate Change (IPCC) (IPCC, 2019). Semi-empirical bookkeeping models combine land-use change data with predefined equilibrium carbon densities and carbon response curves to track carbon stock changes in vegetation and soils caused by direct anthropogenic impacts (Hansis et al., 2015; Gasser et al., 2020; Houghton and Castanho, 2023; Qin et al., 2024). In contrast, process-based DGVMs simulate ecosystem responses and estimate F_{LUC} as the difference in net biome productivity between simulations with constant pre-industrial and transient land use, thereby accounting for direct and indirect anthropogenic effects (Sitch et al., 2024; Pongratz et al., 2014). Beyond terminological inconsistencies between the model types, large uncertainties associated with F_{LUC} arise from limitations in input data and modeling assumptions (Pongratz et al., 2021; Obermeier et al., 2025). These include uncertainties in underlying land use and land-use change forcing data (Ganzenmüller et al., 2022; Hartung et al., 2021; Gasser et al., 2020; Houghton and Nassikas, 2017; Houghton and Castanho, 2023), vegetation and soil carbon densities (Bastos et al., 2021; Hansis et al., 2015), model initialization and complexity (Ganzenmüller et al., 2022; Hartung et al., 2021; Arneth et al., 2017; Bastos et al., 2021), climate forcing (Loughran et al., 2021), and other modeling assumptions (Dorgeist et al., 2024; Houghton and Castanho, 2023; Bastos et al., 2021). Despite this extensive literature, uncertainties related to the spatial distribution and classification quality of vegetation types undergoing land-use change remain almost entirely overlooked, even though these are central in both bookkeeping models and DGVMs.

Multiple approaches have been developed to determine the spatial distribution of vegetation for global modeling. In both bookkeeping models and DGVMs, vegetation types are typically defined based on the concept of Potential Natural Vegetation (PNV). Initially introduced by Tüxen (1956), PNV describes the hypothetical equilibrium state of mature vegetation under prevailing environmental conditions in the absence of direct anthropogenic disturbances. As such, PNV represents the vegetation that would occur under the current climate without any human land use (Chiarucci et al., 2010; Hengl et al., 2018; Champreux et al., 2024). To meet the diverse requirements of different research fields and applications, various classification schemes have been proposed to map global PNV. Widely used examples include the Holdridge life zones (Holdridge, 1967), the global potential vegetation types by Ramankutty and Foley (1999), the global ecoregions and terrestrial biomes (Olson et al., 2001; Dinerstein et al., 2017), and the global ecological zones used for FAO forest reporting (FAO, 2001, 2012).

https://doi.org/10.5194/egusphere-2026-2682
Preprint. Discussion started: 3 June 2026

Existing PNV maps differ in their underlying assumptions, definitions, and class boundaries, limiting their applicability for F_{LUC} assessments. Expert-based PNV mapping approaches (e.g., Olson et al., 2001; Dinerstein et al., 2017; FAO, 2001) are inherently subjective and often combine different regional classifications, which limits consistency, reproducibility, and transparency (Chiarucci et al., 2010; Conradi et al., 2020; Fischer et al., 2022). Remote sensing-based estimates are reproducible but reflect current land cover, which is heavily influenced by anthropogenic activities in many regions. As a result, remote sensing-based PNV maps either depict actual vegetation cover rather than PNV (e.g., Friedl et al., 2010; Higgins et al., 2016) or require additional PNV maps to mask areas affected by land-use change (e.g., Ramankutty and Foley, 1999). Model-based approaches constitute a third major family of PNV mapping methods. These include: correlative models that predict PNV distribution using a limited number of generally climate-focused environmental drivers (e.g., Holdridge, 1967; Whittaker, 1975); process-based models that simulate the ecological or physiological processes governing vegetation distribution (e.g., Arneth et al., 2017; Smith et al., 2014; Kaplan et al., 2003); and data-driven approaches that use vegetation data and environmental variables to derive PNV distribution by training statistical models (e.g., Levavasseur et al., 2012; Hengl et al., 2018; Bonannella et al., 2023b; Beigaitė et al., 2022a). However, model-based approaches simplify the relationship between potential vegetation and environmental drivers and therefore do not fully capture the heterogeneous ecological and historical processes shaping PNV distribution (Champreux et al., 2024). Moreover, correlative and process-based models often deviate from observed vegetation patterns due to insufficient incorporation of empirical data (Bonannella et al., 2023b), and individual models produce highly divergent results because of differences in model structure, complexity, parameterization, input data, and vegetation class definitions (Dallmeyer et al., 2019; Moncrieff et al., 2016). Beyond these approach-specific limitations, most existing PNV maps do not provide a quantification of associated uncertainties, thereby limiting their reliability and applicability (Dietze, 2017; Meyer and Pebesma, 2021). Thus, deriving PNV at high resolution, including associated uncertainty, requires a reproducible framework that integrates representative and robust data on vegetation unaltered by anthropogenic influence while minimizing subjective, expert-based judgments.

Recent developments in PNV mapping increasingly rely on data-driven approaches using machine learning algorithms combined with pollen-based biome reconstructions (Levavasseur et al., 2012; Hengl et al., 2018; Lindgren et al., 2021; Bonannella et al., 2023b) or remote sensing observations (Beigaitė et al., 2022a, b). Within these approaches, the application of machine learning reduces the influence of subjective decisions, enables the integration of a wide range of environmental variables influencing vegetation growth, and is computationally efficient in producing high-resolution maps. Pollen-based biome reconstructions are particularly well suited for predicting PNV, as they provide representative information beyond the actual sampling location, allowing for the reconstruction of biomes from remaining vegetation fragments in landscapes strongly altered by land-use activities (Hengl et al., 2018). In contrast, data-driven approaches based on remote sensing observations depend on training data from areas outside direct human influence. Nevertheless, previous studies using pollen-based biome reconstructions for PNV predictions remain constrained by the limited availability and spatial biases of training data.

https://doi.org/10.5194/egusphere-2026-2682
Preprint. Discussion started: 3 June 2026

Within bookkeeping models and DGVMs, PNV maps play a fundamental role for quantifying F_{LUC}. In these models, PNV is typically represented through so-called Plant Functional Types (PFTs), which are classes of plant species with similar functional traits that respond uniformly to environmental drivers (Moncrieff et al., 2016; Poulter et al., 2015; Wullschleger et al., 2014). In bookkeeping models, PFTs determine key parameters, including the spatial distribution of vegetation and soil carbon densities, the allocation of carbon to different pools, and the residence times of carbon within those pools (Hansis et al., 2015). In DGVMs, changes in PFT distribution alter surface and vegetation properties, thereby influencing simulated water, energy, and carbon fluxes (Harper et al., 2023). Most existing PNV maps are not directly compatible with model requirements, due to different class definitions, degrees of complexity, and spatial resolution, and instead need to be translated into model-specific PFTs. Uncertainties in PNV inputs and processing steps thus propagate directly into derived PFT maps and subsequently affect F_{LUC} estimates. In ecotonal regions, where ecosystems transition between vegetation types such as forests and grasslands, the assumed distribution of PFTs becomes particularly important as F_{LUC} estimates can differ substantially depending on whether abandoned land is assumed to return to grassland or forest. Consequently, analyzing the influence of underlying PFT distributions and associated uncertainties on F_{LUC} estimates is crucial for identifying drivers of F_{LUC} uncertainty and informing future model development.

Here, we assess the sensitivity of F_{LUC} estimates to underlying PNV information by deriving new PFT maps and implementing them in the widely used bookkeeping model BLUE (Bookkeeping of Land Use Emissions; Hansis et al., 2015). The objectives of this study are to (1) develop improved high-resolution PNV maps and quantify associated uncertainties, and (2) assess how variations in PFT distributions propagate into F_{LUC} estimates. Our approach involves compiling an enhanced dataset of pollen-based biome reconstructions and combining it with data on climate, soil, and geomorphology to train an ensemble of random forest classifiers predicting global PNV distributions. The resulting PNV maps are subsequently translated to PFT maps. We derive one best-guess and two sensitivity PFT maps and integrate them into the spatially explicit BLUE model. F_{LUC} estimates from these simulations are compared with estimates based on the default PFT map of BLUE to quantify the sensitivity of F_{LUC} to PNV-related uncertainty. Overall, our approach provides a practical framework for predicting PNV distributions and translating them into PFT maps and is applicable to other bookkeeping models and DGVMs that rely on such data.

2 Data and methods

The following chapter first describes the preparation of the pollen-based biome reconstructions used as training data and the machine learning approach for predicting global PNV maps. It subsequently introduces the BLUE model, the reclassification framework linking the PNV predictions to PFTs, and the simulation set-up. A schematic overview of the workflow is provided in Fig. 1. An overview of the input datasets is given in the Supplement: Table S1 lists the biome datasets, Table S2 lists the environmental predictors used for machine learning, and Table S3 lists additional datasets used to prepare the training data, define the spatial extent of PNV predictions, and reclassify the PNV classes into PFTs. The preparation of environmental predictors and additional datasets is described in Supplementary Text S1.1.

https://doi.org/10.5194/egusphere-2026-2682
Preprint. Discussion started: 3 June 2026

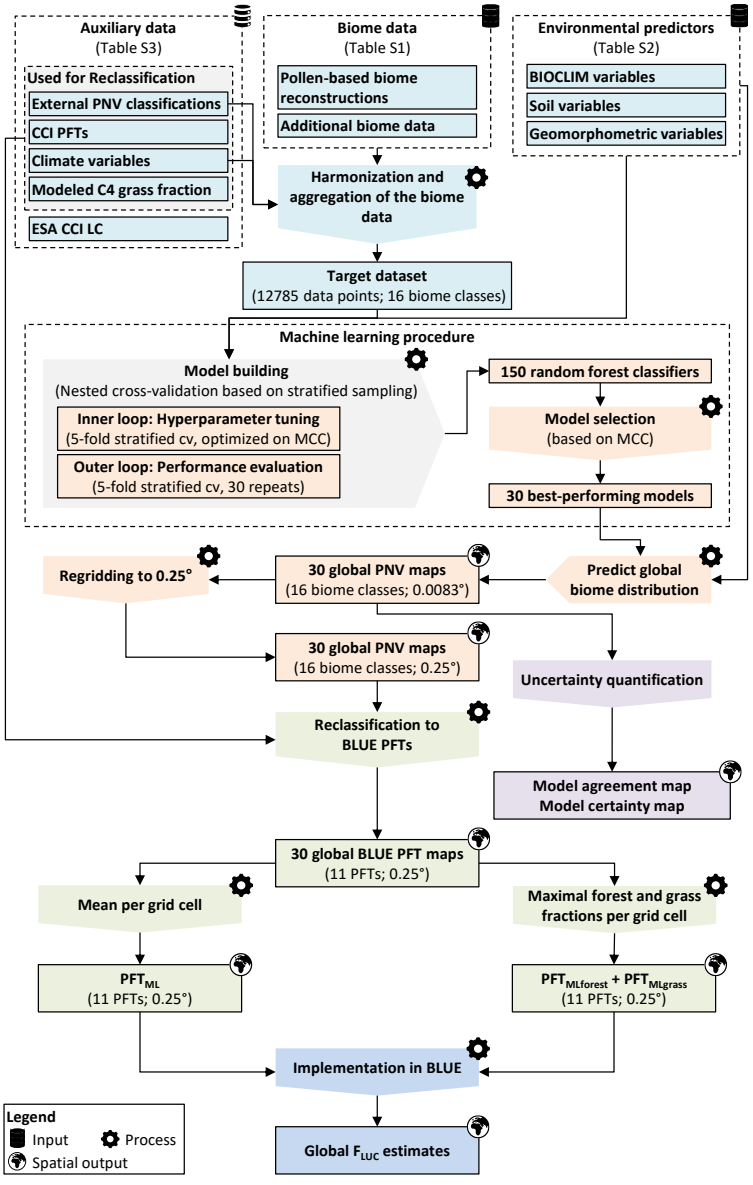

Figure 1. Schematic workflow illustrating the main input data, processing steps, and outputs of our approach. The processing steps include the generation of potential natural vegetation (PNV) maps from pollen-based biome reconstructions, their reclassification into PFT maps, and the implementation of these PFT maps in the bookkeeping model BLUE for estimating the net carbon dioxide (CO_2) flux from land use and land-use change (F_{LUC}). Comprehensive lists of input datasets are provided in Tables S1–S3.

https://doi.org/10.5194/egusphere-2026-2682
Preprint. Discussion started: 3 June 2026

2.1 Compilation of pollen-based biome reconstructions

We compile training data for the global PNV predictions from present-day pollen-based biome reconstructions. Our primary source is the BIOME 6000 database (Harrison, 2017), which harmonizes data from 17 regional studies into a single classification scheme with 32 biome classes. The biomes of individual data points are reconstructed based on pollen samples found in sediments, moss polsters, soil, and other deposits according to the approach described by Prentice et al. (1996). In addition to the BIOME 6000 database, we adopt expansions by Hengl et al. (2018) (also used in Bonannella et al., 2023b), adding data for the Eastern Mediterranean, Black Sea, and Caspian Sea regions (Marinova et al., 2018) and Brazil (Veloso et al., 1992). We further include regional datasets for Eurasia (Binney et al., 2017), China (Sun et al., 2020), the Tibetan Plateau (Qin et al., 2022), and South America (Flantua et al., 2015).

Individual biome datasets are processed, verified for plausibility, and harmonized to create a consistent training dataset, i.e., for multiple pollen samples at the same location, only the most frequent biome is selected. As pollen from intensively managed agricultural land may be misclassified as tundra (Binney et al., 2017), tundra data points are only retained at ecologically plausible locations (see Supplementary Text S1.2 for details). The regional biome reconstructions by Sun et al. (2020) and Qin et al. (2022) use a different biome classification scheme with 18 biome classes and are therefore converted to the 32 biome classes used by the BIOME 6000 database (Table S4). At overlapping sites, BIOME 6000 data points are discarded in favor of regional datasets.

We aggregate the 32 BIOME 6000 classes into 16 biome classes, as the original classes are too location-specific and detailed, resulting in insufficient class observations for global modeling tasks (Bonannella et al., 2023b). The aggregation to 16 classes supports (1) the definition of biome classes suitable for machine learning, with classes that are large enough for training and distinguishable by environmental characteristics, and (2) achieving a balance between generalization and ecological detail for global modeling. The 16 biome classes are defined based on matching plant form (grasses, shrubs, trees), leaf type (broadleaf, needleleaf), phenology (evergreen, deciduous), and climate region (tropical, warm-temperate, temperate/boreal) (Table S5).

The final biome data for the global PNV predictions consist of 12 785 data points from 12 404 unique locations, classified into 16 biomes (compare Fig. 2a). The number of unique biome locations represents an increase of 86% compared to Levavasseur et al. (2012) (6 691 locations) and 54% compared to Hengl et al. (2018) and Bonannella et al. (2023b) (8 057 locations). The mismatch between the number of data points and unique locations arises because we retain all corresponding biomes when multiple biomes are equally common at a location. Despite our efforts to increase the number of data points, the sampling points are spatially clustered and large areas, especially in Africa and Australia, remain sparsely sampled. Additionally, biome class sizes remain imbalanced, ranging from 152 observations for “Sclerophyll woodland and shrubland” to 2 277 observations for “Temperate/boreal mixed forest” (Table 1).

https://doi.org/10.5194/egusphere-2026-2682
Preprint. Discussion started: 3 June 2026

2.2 Global PNV prediction with random forest classifiers

We employ random forest classifiers to predict the global PNV distribution at $0.0083°$ spatial resolution (commonly referred to as $1\,\mathrm{km}$ resolution). For this multiclass classification task, we utilize the prepared pollen-based biome data as the response variable and a stack of 25 environmental variables as predictors. Random forest classifiers are well-suited for spatial prediction tasks, such as ecological modeling and land cover classification, due to their computational efficiency, robustness to outliers and noise, minimal preprocessing needs, and ability to handle complex, unbalanced data (Meyer et al., 2019; Rodriguez-Galiano et al., 2012; Wulder et al., 2018; Yang and Huang, 2021; Beigaitė et al., 2022a; Sidumo et al., 2022). They outperform other classification algorithms in regional species modeling (Bonannella et al., 2022) and pollen-based biome reconstructions at continental to global scales (Sobol and Finkelstein, 2018; Hengl et al., 2018). The predictors comprise data on climate, soil, and topography, and thus encompass typical environmental drivers that govern vegetation appearance and composition. The final predictors are chosen based on their relevance for vegetation growth, the absence of direct anthropogenic influences, and the public availability of global data at a spatial resolution equal to or higher than $0.0083°$ to provide high-resolution PNV maps (Ganzenmüller et al., 2025).

We implement a nested cross-validation to ensure an unbiased assessment of model performance and generalization to new observations (Bischl et al., 2023). This involves an inner stratified 5-fold cross-validation dedicated to hyperparameter tuning, for which we use a grid search approach to optimize hyperparameter values (see Table S6 for the hyperparameter space and values). An outer stratified 5-fold cross-validation with 30 repeats then provides an unbiased evaluation on unseen data. The stratified sampling is crucial to ensure proportional representation of biome classes across all folds, which is particularly important for imbalanced datasets (Lyons et al., 2018; Kohavi, 1995). The model-building procedure results in 150 trained models, of which we select the 30 top-performing models (20% of all trained models) to create 30 global PNV maps, which are then used in all subsequent processing steps. The cutoff point at 20% is chosen as a compromise to ensure reliable predictions while maintaining computational efficiency.

As a primary metric to assess the overall and per-class predictive performance of the trained models, we use the Matthews correlation coefficient (MCC; Pedregosa et al., 2011). It directly evaluates the predicted class values of the hard classifier (i.e., the biome classes), considers all entries in the confusion matrix (which indicates the performance of the machine learning classification), and is well-suited for the evaluation of imbalanced datasets with different class sizes (Bekkar et al., 2013; Chicco and Jurman, 2020; Jurman et al., 2012). The MCC values range from -1 to +1, where +1 indicates perfect classification, 0 random predictions, and -1 perfect misclassification (Jurman et al., 2012). Additionally, the overall MCC is chosen as the optimization criterion during hyperparameter tuning and for the selection of the 30 top-performing models. We further compute the R^2_{logloss} (Bonannella et al., 2022) and other commonly used classification metrics, such as the overall accuracy as well as per-class precision and recall (Pedregosa et al., 2011).

https://doi.org/10.5194/egusphere-2026-2682
Preprint. Discussion started: 3 June 2026

The spatially explicit uncertainty associated with the global PNV predictions is provided through two metrics: (1) model agreement, calculated as the proportion of models that assign the biome class predicted by the majority of models (henceforth referred to as "majority class"), (2) model certainty, calculated as the average predicted probability of the majority class across all models. Model agreement represents the uncertainty caused through the different training data subsets, whereas model certainty refers to the internal model uncertainty, based on the confidence of the random forest classifiers.

2.3 The bookkeeping model BLUE

The spatially explicit bookkeeping model BLUE estimates F_{LUC} by tracking carbon stock changes in vegetation, soil, harvested wood products, and the atmosphere following land-use change events (Hansis et al., 2015). BLUE distinguishes four land cover types (primary land, secondary land, cropland, and pasture) and 11 PFTs representing the PNV that constitutes primary and secondary land. The model further considers the following land-use activities: abandonment (change from cropland or pasture to secondary land), clearing (change from primary land or secondary land to cropland or pasture), wood harvest (change from primary to secondary land or land management on secondary land), and transitions between cropland and pasture. Following a land-use activity, BLUE tracks changes in carbon pools (i.e., vegetation, soil, harvested wood products, and atmosphere) based on response curves specific to each PFT and land cover type. In BLUE, F_{LUC} is derived as the annual change in the atmospheric carbon pool. The default PFT map used in BLUE is created by aggregating the 15 classes from the PNV map by Ramankutty and Foley (1999) into the 11 BLUE PFT classes using fixed allocation rules based on predefined bioclimatic and geographical thresholds, followed by regridding to a spatial resolution of $0.5°$ (Pongratz et al., 2008). The underlying PNV map of Ramankutty and Foley (1999) is largely based on remote sensing observations, with areas dominated by anthropogenic land use masked by an expert-based PNV map composite published in Haxeltine and Prentice (1996).

2.4 Reclassification to BLUE PFTs

For implementation in the BLUE model, the 30 global PNV maps are first regridded to a spatial resolution of $0.25°$ to match the resolution of other input datasets used in BLUE. These regridded maps are then reclassified into the 11 BLUE PFTs (six forest PFTs, two shrub PFTs, two grass PFTs, and one tundra PFT). We apply a spatially explicit reclassification scheme to translate each of the 30 global PNV maps into PFT maps (Table S7). Some biome classes (ID 1, 3, 5, 6, 7, 16; see Table S7) are directly assigned to specific BLUE PFTs, whereas mixed biome classes are fractionally allocated among relevant BLUE PFTs because they cannot be represented by a single PFT. This fractional allocation relies on additional spatially explicit datasets that quantify the grid-cell fractions of important vegetation traits, including plant form (grasses, shrubs, trees), leaf type (broadleaf, needleleaf), phenology (evergreen, deciduous), and climate region (tropical, temperate) (see Supplementary Text S1.3 for details). Global grid-cell fractions of plant form, leaf type, and phenology are obtained from the PFT dataset by Harper et al. (2023) (henceforth referred to as CCI PFTs), which is based on ESA CCI land cover dataset (Copernicus Climate Change Service, 2019). Following Beigaitė et al. (2022b) and Dallmeyer et al. (2019), anthropogenic land-use change is assumed to replace vegetation types proportionally. Accordingly, the relative proportions of the tree, shrub, and natural grass CCI PFTs are used as proxies for vegetation traits under PNV conditions. For mixed biome classes without explicitly defined climate regions, tree

https://doi.org/10.5194/egusphere-2026-2682
Preprint. Discussion started: 3 June 2026

and shrub fractions are allocated to tropical or temperate BLUE PFTs according to the grid-cell fractions of tropical vegetation in the Holdridge life zones (Elsen et al., 2022) and the 2010 update of the global ecological zones (FAO, 2012) (Fig. S1a). Grass fractions are split into the BLUE PFTs "C3 natural grasses" and "C4 natural grasses" using grid-cell-specific C4 grass fractions (Fig. S1b), primarily derived from Luo et al. (2024) and complemented by the cross-over temperature approach of Griffith et al. (2015). Grid-cell fractions of non-vegetated surface cover are estimated by summing all abiotic grid-cell fractions from the CCI PFTs (Harper et al., 2023), which include permanent inland water bodies, permanent snow and ice cover, and bare soil. Grid cells classified as completely non-vegetated according to the ESA CCI land cover dataset (Copernicus Climate Change Service, 2019) are treated as fully abiotic (see Supplementary Text S1.1). As the PFT classes used in BLUE are similar to those employed in other bookkeeping models and DGVMs, our PFT maps can be translated through cross-walking tables or the reclassification approach itself can be adapted to accommodate alternative PFT classifications.

Using the reclassification scheme, we translate the 30 PNV maps into 30 PFT maps consistent with the BLUE PFT definitions. The ensemble mean of these 30 PFT maps is used as best-guess estimate (PFT_{ML}). To assess the PNV-related uncertainty in F_{LUC} estimates, we derive two sensitivity maps ($PFT_{MLforest}$ and $PFT_{MLgrass}$). To create $PFT_{MLforest}$ and $PFT_{MLgrass}$, PFT values are assigned for each grid cell based on the maximum predicted forest fraction (sum of the six forest PFTs) and grass fraction (sum of the two grass PFTs), respectively, across the 30 PFT maps. Because forests and grasses often represent opposite ends of the parameter ranges in BLUE (e.g., for vegetation carbon densities), maximizing these PFT categories provides plausible upper and lower bounds of the predicted values. The two sensitivity maps are therefore used to approximate the maximum spread of simulated F_{LUC} and to quantify how uncertainties in PNV maps propagate into F_{LUC} estimates.

2.5 BLUE simulations

We run four BLUE simulations using different PNV maps: (1) PFT_{Hansis}, (2) PFT_{ML}, (3) $PFT_{MLforest}$, and (4) $PFT_{MLgrass}$. PFT_{Hansis} refers to the default PFT map of BLUE, whereas the other three labels refer to the respective PFT maps created in this study. All simulations are initialized in 1700 and follow the land-use trajectories from the LUH2-GCB2024 dataset (Friedlingstein et al., 2025; Chini et al., 2021).

3 Results

3.1 Global PNV predictions

The global PNV distribution of the 16 biome classes, derived from the ensemble mean of the 30 random forest classifiers, reflects expected large-scale biome patterns (Fig. 2). These patterns largely follow the spatial distribution of the underlying training data: "Tropical evergreen rainforest" along the equator transitioning into "Tropical savannas", and "Deserts" and "Xerophytic woods/shrubs" dominating arid regions. The mid-latitudes are characterized by a mix of temperate forest types and the "Steppe" biome. Boreal climate zones, in contrast, contain large areas of "Temperate/boreal evergreen conifers". Some biome

https://doi.org/10.5194/egusphere-2026-2682
Preprint. Discussion started: 3 June 2026

classes, such as “Temperate/boreal evergreen conifers” and “Steppe”, are widespread, whereas others, including “Sclerophyll woodland and shrubland” and “Evergreen needleleaf open woodland”, are restricted to smaller areas.

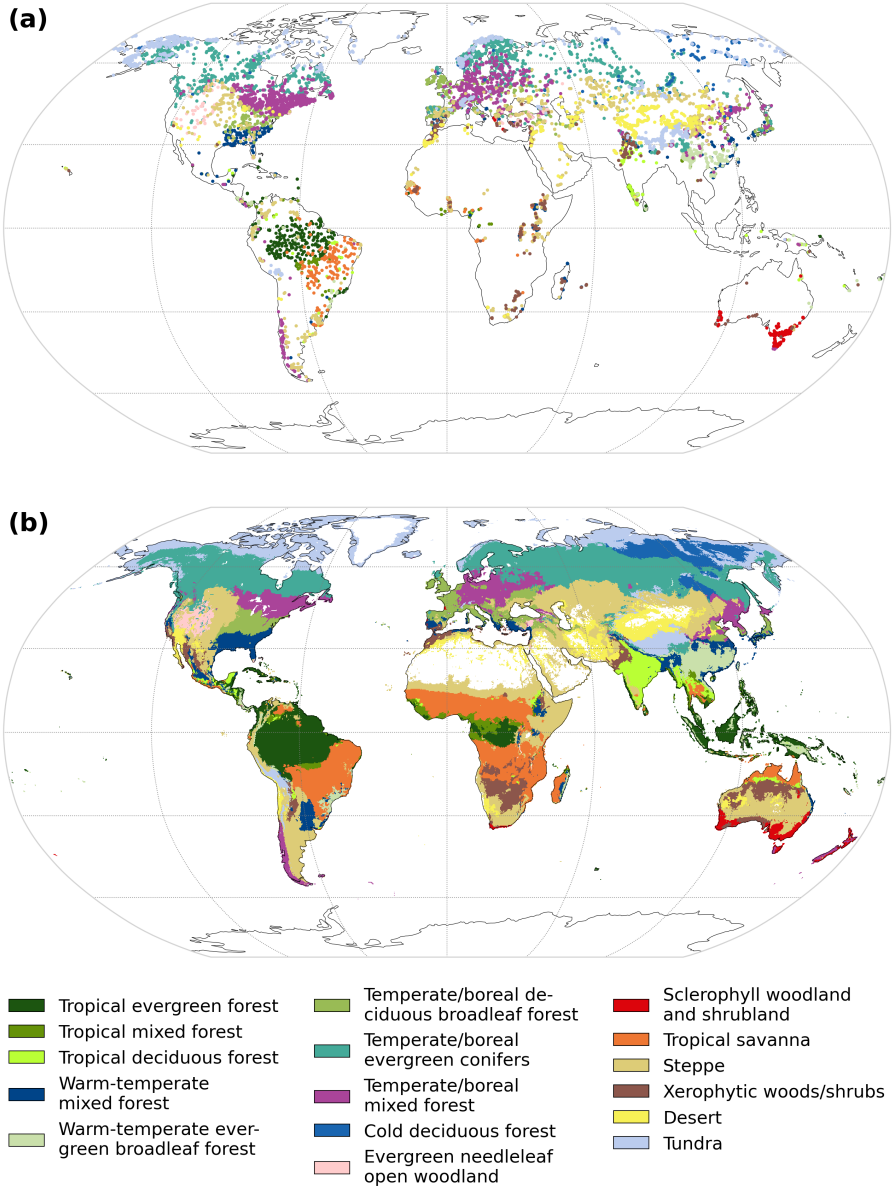

Figure 2. Global maps of (a) biome data points used as training data and (b) predicted distribution of potential natural vegetation (PNV) biome classes. Grid cells in (b) show the majority vote of the 30 top-performing models on the biome class with the highest fractional coverage across the regridded global PNV maps at 0.25° spatial resolution.

https://doi.org/10.5194/egusphere-2026-2682
Preprint. Discussion started: 3 June 2026

The random forest classifiers generally demonstrate robust performance in predicting the global PNV distribution (Table 1), on average achieving an overall MCC of 0.67, a classification accuracy of 0.71, and an R^2_{logloss} of 0.65. Average predictive performance varies among the 16 biome classes, with the highest MCC observed for "Warm-temperate evergreen broadleaf forest" (0.82) and "Tundra" (0.77), whereas "Tropical mixed forest" (0.41) and "Xerophytic woods/shrubs" (0.42) exhibit the lowest MCC values. Predictions for larger biome classes have a lower variance in their predictive performance (Fig. S2), however, class size alone is not the sole determinant of model performance. Smaller biome classes such as "Sclerophyll woodland and shrubland" (n=152) and "Tropical evergreen rainforest" (n=402) have comparatively high MCC values (0.76 and 0.75, respectively), likely reflecting a combination of distinct environmental characteristics associated with these biomes and a positive bias due to spatial autocorrelation. Precision and recall estimates provide insight into potential misclassifications of biome classes (Table 1). For example, "Cold deciduous forest" and "Evergreen needleleaf open woodland" show higher precision (0.65 and 0.64, respectively) than recall (0.46 and 0.46, respectively), suggesting an under-representation of those biome classes in the predictions due to misclassifications into other biome classes. In contrast, biome classes with higher recall than precision, such as "Tropical savanna", are likely overrepresented in the prediction. In this case, the random forest classifiers correctly predict a larger proportion of true instances, resulting in a higher recall (0.72) but at the cost of lower precision (0.62) due to increased misclassifications. The four largest biome classes ("Temperate/boreal mixed forest", "Temperate/boreal evergreen conifers", "Temperate/boreal deciduous broadleaf forest", and "Steppe") exhibit lower R^2_{logloss} values relative to their MCC, precision, and recall values, indicating that random forest classifiers have lower confidence in the underlying class probabilities than their class predictions suggest. We assume that this effect is driven by a combination of the large geographical extent of these widespread biomes and the imbalanced dataset. The broad extent increases heterogeneity in environmental characteristics, lowering the predicted probability, whereas class imbalance leads to comparatively higher performance for discrete class predictions of large biome classes.

Maps for model agreement and certainty among the 30 models provide an overview of prediction reliability (Fig. 3). Model agreement, reflecting uncertainty arising from the use of different data subsets during model training, is high (> 80%) across 89% of the vegetated land surface (Fig. 2a). This suggests that variations in the training data subsets exert only limited influence on the predicted biome distribution. However, model agreement drops notably in transitional zones between biome classes, such as the interface between "Temperate/boreal mixed forest" and "Temperate/boreal evergreen conifers" in eastern Europe. In contrast, model certainty, reflecting the internal model uncertainty based on the confidence of the random forest classifiers in their class predictions, is considerably lower, with only 21% of the vegetated land surface showing a model certainty > 80% (Fig. 3b). This indicates that consistent predictions across models do not necessarily imply strong confidence in the predicted biome class. Areas with low model certainty (< 40%) often occur in transitional zones, but also coincide with regions sparsely represented in the training dataset. These include extensive areas in Australia, Africa, Mexico and Central America, southern Brazil, and Bangladesh, where complex environmental conditions, such as mountainous terrain, subtropical moist climates, or arid zones, additionally limit model generalization. Conversely, regions such as lowland Sumatra and Borneo show relatively

https://doi.org/10.5194/egusphere-2026-2682
Preprint. Discussion started: 3 June 2026

Table 1. Average predictive performance of the 30 best-performing random forest classifiers for each biome class and overall, quantified using the Matthews correlation coefficient (MCC), precision, and recall. In addition, the table reports the number of observations (N. obs) for each biome class and the training dataset. Overall metrics are calculated by micro-averaging, giving each sampling location the same contribution to the overall score.

Biome class	**N. obs**	**MCC**	**Precision**	**Recall**	$\mathbf{R^2_{logloss}}$
Tropical evergreen forest	402	0.75	0.73	0.79	0.74
Tropical mixed forest	193	0.41	0.48	0.37	0.52
Tropical deciduous forest	216	0.46	0.54	0.42	0.54
Warm-temperate mixed forest	792	0.54	0.57	0.57	0.51
Warm-temperate evergreen broadleaf forest	664	0.82	0.81	0.85	0.77
Temperate/boreal deciduous broadleaf forest	1456	0.63	0.65	0.71	0.52
Temperate/boreal evergreen conifers	2110	0.74	0.78	0.78	0.60
Temperate/boreal mixed forest	2277	0.71	0.76	0.75	0.56
Cold deciduous forest	227	0.53	0.65	0.46	0.52
Evergreen needleleaf open woodland	275	0.53	0.64	0.46	0.54
Sclerophyll woodland and shrubland	152	0.76	0.75	0.78	0.70
Tropical savanna	291	0.66	0.62	0.72	0.66
Steppe	1356	0.59	0.62	0.65	0.45
Xerophytic woods/shrubs	389	0.42	0.47	0.41	0.47
Desert	644	0.70	0.76	0.66	0.63
Tundra	1341	0.77	0.77	0.82	0.69
Overall	12785	0.67	0.71	0.71	0.65

high certainty despite a lack of training data, likely due to similar environmental conditions well-represented elsewhere in the training data.

3.2 Differences in PFT distributions

According to the best-guess PFT map (PFT_{ML}), the PNV of the global vegetated land surface consists of 59% forest PFTs, 32% grass PFTs, 5% tundra PFT, and 4% shrub PFTs (Table S8). The PFT "Temperate/boreal evergreen conifers" covers the largest area, accounting for about 20% of the vegetated land surface, followed by the two grass PFTs (C4: 18%; C3: 14%) and "Tropical evergreen forest" (14%). "Summergreen shrubs" have the lowest extent, covering less than 1% of the vegetated land surface, mainly in semi-arid regions. Besides vegetated land, the abiotic surface cover comprises approximately one-third of the global land surface, mostly in Antarctica, Greenland, and desert regions.

https://doi.org/10.5194/egusphere-2026-2682
Preprint. Discussion started: 3 June 2026

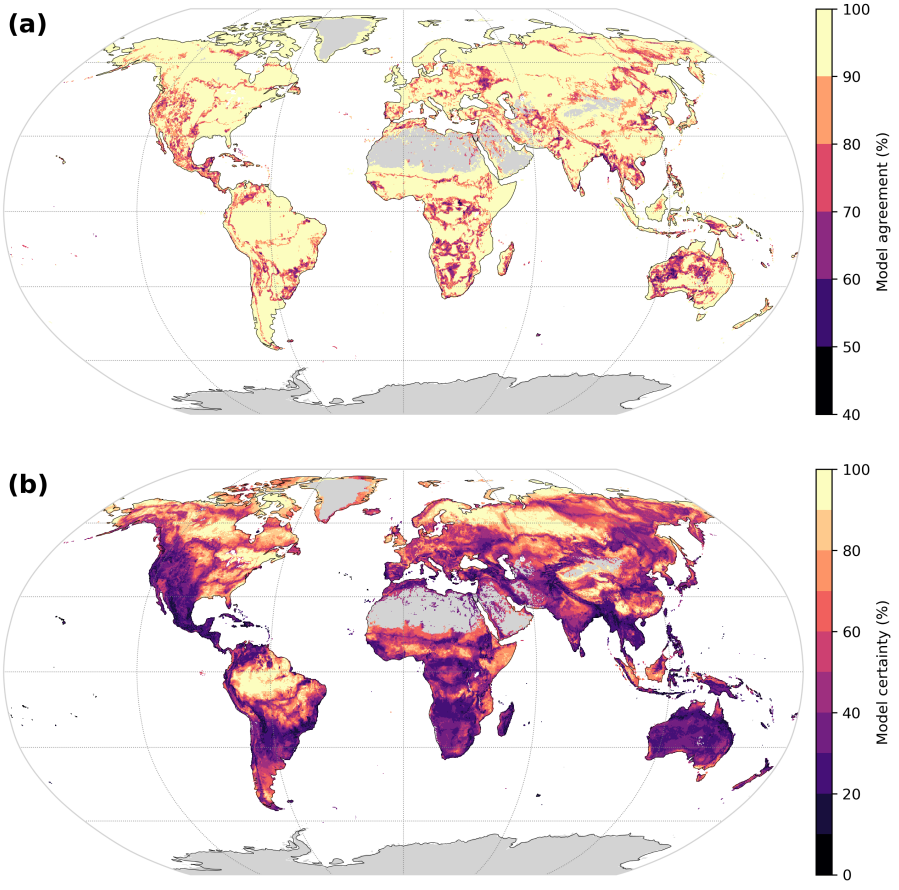

Figure 3. Spatial distribution of (a) model agreement and (b) model certainty for the global potential natural vegetation (PNV) predictions. Model agreement is calculated as the proportion of the 30 best-performing models that predict the majority biome class for each grid cell. Model certainty (b) is derived as the average predicted probability of the majority class for each grid cell across the model ensemble. Lower values of model agreement and certainty indicate higher uncertainty in the PNV classification, and vice-versa. Both model agreement and model certainty are regridded to $0.25°$ spatial resolution for visualization.

The spatial patterns of the best-guess PFT map (Fig. 4; Fig. S3 for individual PFTs) generally follow the distribution of the global PNV predictions (Fig. 2b). The reclassification scheme used to translate the 16 biome classes of the PNV predictions into the 11 PFTs of BLUE effectively captures ecological differences within mixed biome classes, leading to different PFT proportions in areas with the same biome class. For example, the allocation of the biome class "Tropical savanna" to PFTs results in a comparatively high share of forest PFTs in the central African savanna, which diminishes with increasing distance from the equator. In contrast, "Tropical savanna" in eastern Brazil is characterized by a large proportion of the PFT "Raingreen shrubs", whereas in Madagascar it is predominantly assigned to grass PFTs.

https://doi.org/10.5194/egusphere-2026-2682
Preprint. Discussion started: 3 June 2026

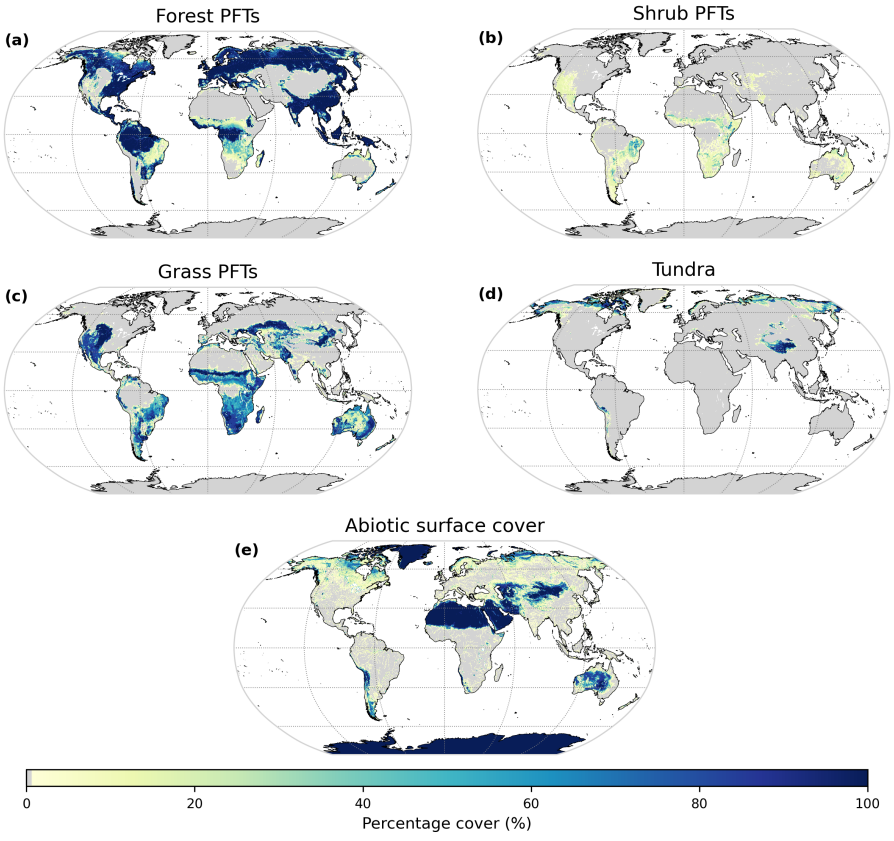

Figure 4. Spatial distribution of the percentage cover of plant functional type (PFT) categories of the best-guess PFT map (PFT_{ML}). The PFT categories are: (a) forest PFTs (sum of IDs 1–6), (b) shrub PFTs (sum of IDs 7–8), (c) grass PFTs (sum of IDs 9–10), (d) tundra (ID 11), and (e) abiotic surface cover. PFT names and corresponding IDs are provided in Table S8. Grid cells with zero percentage cover are colored grey. The spatial distribution of the percentage cover of the individual PFTs of the best-guess PFT map is displayed in Fig. S3.

The best-guess PFT map and the default PFT map of BLUE (Fig. S4) show substantial differences in both spatial distribution and total PFT areas (Fig. S5, Table S8). In the best-guess PFT map, forest PFTs cover 20% more area than in the default PFT map, primarily at the expense of shrub PFTs, whose total area is reduced by 74%. In contrast, the total area covered by grass PFTs remains similar between the two PFT maps. The largest discrepancy for an individual PFT is observed for "Raingreen shrubs", whose area is 79% smaller in the best-guess PFT map. Even where total area estimates are similar, spatial distributions of individual PFTs can differ substantially between the two maps, as is particularly evident for the grass PFTs "C3 natural grasses" and "C4 natural grasses" (Fig. S5). Similarly, despite comparable global extents, the spatial distribution of abiotic surface cover varies in many areas. The best-guess PFT map assigns larger abiotic surface cover fractions across many arid to semi-arid regions, including Australia, Central Asia, and the Middle East, whereas the default PFT map shows greater abiotic

https://doi.org/10.5194/egusphere-2026-2682
Preprint. Discussion started: 3 June 2026

surface cover in boreal latitudes and the American Cordillera.

We further analyze the potential variability in PFTs by constructing two sensitivity maps: one with maximum forest extent ($PFT_{MLforest}$) and one with maximum grass extent ($PFT_{MLgrass}$). Due to the construction method, $PFT_{MLforest}$ has higher forest and a lower grass fraction compared to the best-guess PFT map (PFT_{ML}), whereas the opposite pattern is observed for $PFT_{MLgrass}$. The largest spatial differences between $PFT_{MLforest}$ and $PFT_{MLgrass}$ occur in transitional zones between forest- and grass-dominated biome classes, such as the border regions of "Steppe" in Eurasia and North America and "Tropical savanna" in northern Australia and southern Brazil (Fig. S6).

3.3 F_{LUC} estimates based on varying PFT maps

Global net F_{LUC} estimates derived with the bookkeeping model BLUE reveal substantial differences between simulations using the PFT maps from this study (PFT_{ML}, $PFT_{MLforest}$, $PFT_{MLgrass}$) and the simulation based on the default PFT map of BLUE (PFT_{Hansis}). Using the best-guess PFT map, cumulative net F_{LUC} estimates for the period 1850–2023 amount to $292\,\mathrm{PgC}$, which is 16% higher than the $252\,\mathrm{PgC}$ estimated with the default PFT map. Simulations using the sensitivity maps from this study estimate cumulative F_{LUC} of $319\,\mathrm{PgC}$ under maximum forest extent ($PFT_{MLforest}$) and $266\,\mathrm{PgC}$ under maximum grass extent ($PFT_{MLgrass}$), corresponding to increases of 27% and 6%, respectively, compared to the default simulation. The resulting spread of $53\,\mathrm{PgC}$ between the simulations of the two sensitivity maps exceeds the $40\,\mathrm{PgC}$ difference observed between the simulations using the best-guess PFT map and the default PFT map. Over time, global net F_{LUC} estimates exhibit similar temporal trajectories across all four simulations (Fig. 5a), as they are driven by the same land-use data. In all simulations, global F_{LUC} peaks in 1959, followed by a decline and convergence after 2000. However, the F_{LUC} time series derived from the best-guess PFT map consistently shows higher estimates than those based on the default PFT map.

Similar to global net F_{LUC}, the temporal evolution of the individual F_{LUC} component fluxes is largely consistent across the four simulations using different PFT maps (Fig. 5b). In line with previous F_{LUC} estimates (Friedlingstein et al., 2025), emissions from deforestation, including permanent deforestation for agricultural expansion and deforestation associated with shifting cultivation, are the dominant carbon source in all four simulations and most pronounced during the mid-20th century. Larger forest fractions in the best-guess and $PFT_{MLforest}$ maps lead to amplified deforestation emissions relative to the simulation using the default PFT map. By contrast, forest regrowth following agricultural abandonment and as part of shifting cultivation cycles represents the primary carbon sink. Differences in forest regrowth fluxes between the simulations emerge in the 1940s and increase over time, reflecting differences in post-abandonment recovery linked to PFT allocation. As a result, carbon uptake from forest regrowth is higher in the simulations with greater forest PFT cover (PFT_{ML} and $PFT_{MLforest}$). Fluxes from wood harvest (e.g., decay of slash and wood products, regrowth following harvest) and from other land-use transitions (e.g., conversions between crop and pasture) are comparatively similar across the four simulations. Wood harvest fluxes increase slightly over time, whereas fluxes from other land-use transitions remain relatively stable. Overall, the higher net F_{LUC} estimates under the best-guess PFT map compared to the default PFT map largely stem from increased deforestation emissions,

https://doi.org/10.5194/egusphere-2026-2682
Preprint. Discussion started: 3 June 2026

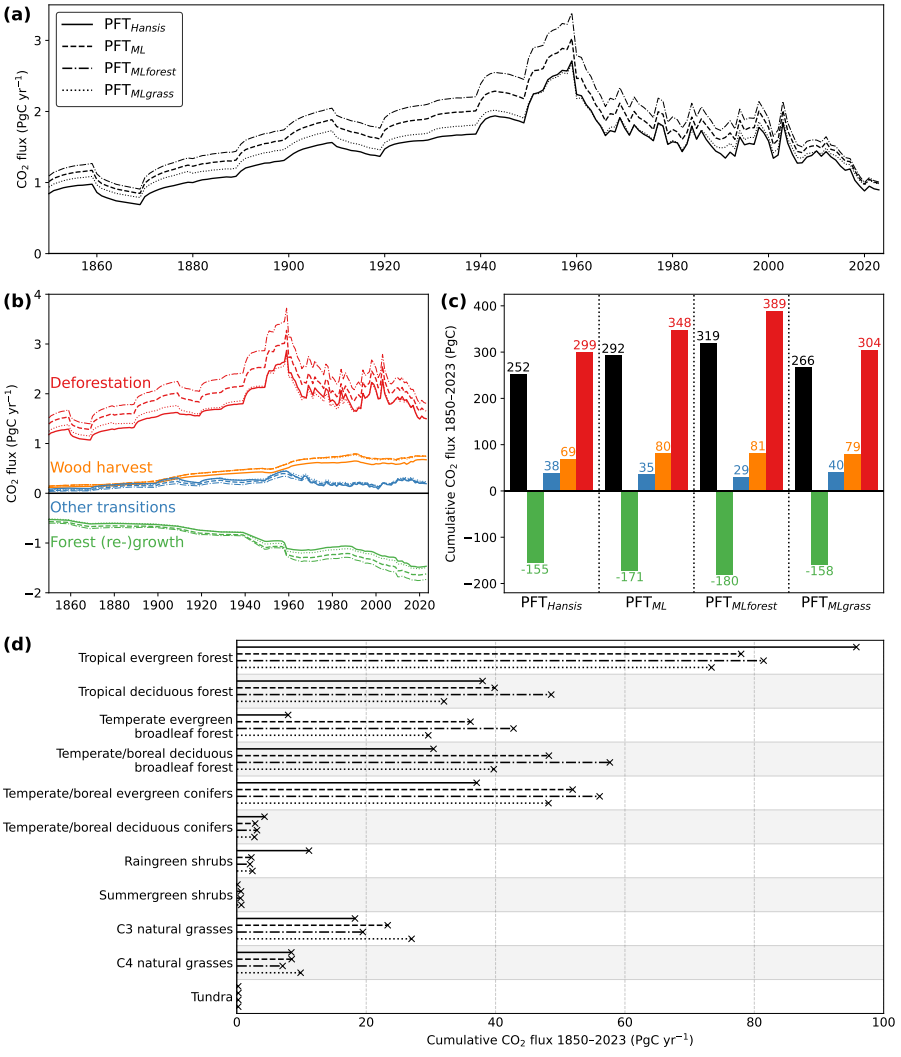

Figure 5. Estimates of the global net carbon dioxide (CO_2) flux from land use and land-use change (F_{LUC}) for the period 1850–2023 derived from the bookkeeping model BLUE. Simulation names refer to the underlying plant functional type (PFT) maps: PFT_{Hansis} (default PFT map of BLUE), PFT_{ML} (best-guess PFT map from this study), and the sensitivity maps from this study $PFT_{MLforest}$ and $PFT_{MLgrass}$, representing maximum forest and grassland extent, respectively (see Sect. 2). (a) Annual F_{LUC} estimates ($PgC\ yr^{-1}$). (b) Annual F_{LUC} estimates ($PgC\ yr^{-1}$) split into component fluxes: (i) carbon emissions from deforestation (red), (ii) carbon removals from forest (re-)growth (green), (iii) carbon fluxes from wood harvest and other forest management (orange), and (iv) carbon fluxes from other land-use transitions (blue). (c) Cumulative (1850–2023) estimates (PgC) of F_{LUC} and component fluxes. (d) Cumulative (1850–2023) F_{LUC} estimates (PgC) attributed to the individual PFTs.

which are only partly offset by higher removals from forest regrowth (Fig. 5c).

https://doi.org/10.5194/egusphere-2026-2682
Preprint. Discussion started: 3 June 2026

Although the broad spatial patterns of F_{LUC} are similar across the four simulations, various regions show major differences (Fig. 6, Figs. S7–S11). Across all simulations, cumulative F_{LUC} between 1850 and 2023 is highest in tropical regions, particularly in Brazil, Central America, West Africa, Ethiopia, and Southeast Asia, as well as in the central United States (Fig. S7). In the more recent period (2000–2023), net emission hotspots are concentrated primarily in the tropics, whereas large areas of temperate regions exhibit net carbon removals (Fig. S8). Between the simulations using the best-guess PFT map and the default PFT map, pronounced discrepancies in F_{LUC} are located in regions with divergent PFT allocations and intense land-use activities (Fig. 6a, Fig. S9a). These differences are particularly evident where the PFT maps disagree on the relative distribution of grass and forest PFTs (Fig. S6).

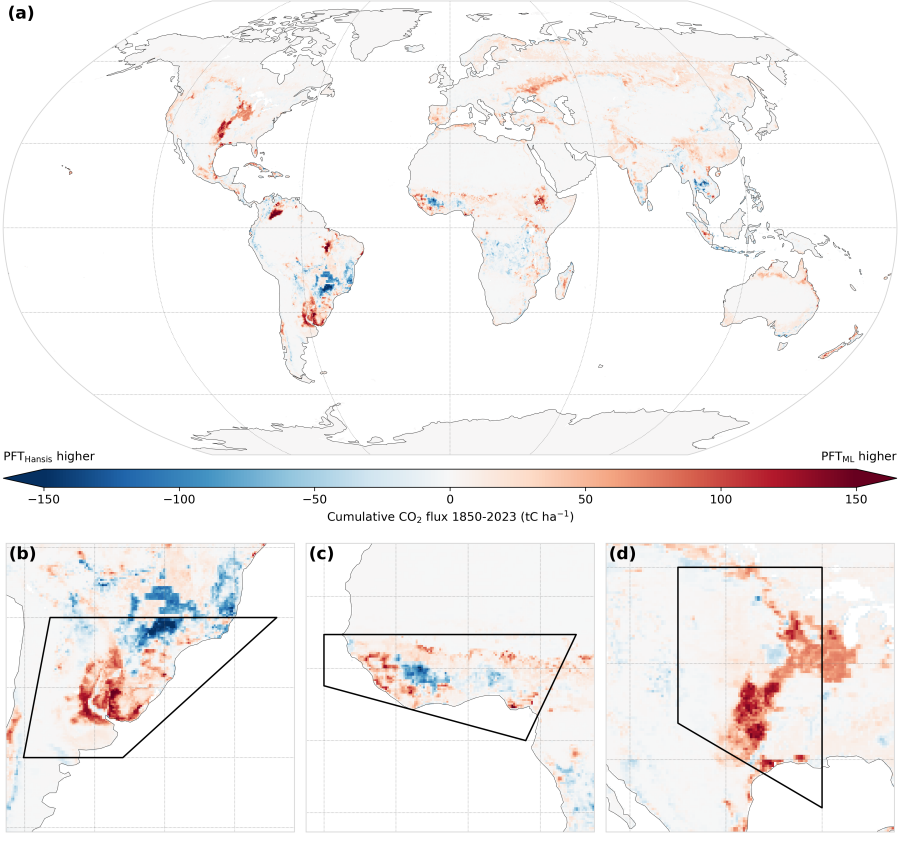

Figure 6. Differences between cumulative (1850–2023) net land use and land-use change flux (F_{LUC}) estimates ($tC\,ha^{-1}$) derived from the bookkeeping model BLUE using the plant functional type (PFT) maps PFT_{Hansis} and PFT_{ML}. PFT_{Hansis} refers to the default PFT map of BLUE, whereas PFT_{ML} refers to the best-guess PFT map from this study. Panel (a) shows the global distribution of cumulative F_{LUC} differences, whereas panels (b)–(d) provide insets for IPCC regions with large cumulative differences discussed in the main text: (b) Southeastern South America (SES), (c) Western Africa (WAF), and (d) Central North America (CNA).

https://doi.org/10.5194/egusphere-2026-2682
Preprint. Discussion started: 3 June 2026

One region with remarkable grid-cell-level differences is Southeastern South America (IPCC region SES; Fig. 6b; IPCC regions are shown in Fig. S12), where F_{LUC} estimates vary considerably between BLUE simulations using the best-guess and the default PFT map. In the northern part of this region, F_{LUC} estimates based on the best-guess PFT map are substantially lower than those based on the default PFT map (blue colors in Fig. 6b). These areas of lower F_{LUC} coincide with grid cells classified as "Tropical savanna" in the PNV predictions and are subsequently assigned predominantly to "C4 grasses" in the best-guess PFT map, whereas they are designated as "Tropical deciduous forest" in the default PFT map. Conversely, in the central part of the SES region the best-guess PFT map assigns a greater fraction of forest PFTs than the default PFT map, leading to higher F_{LUC} in the simulation using the best-guess PFT map. This spatial disagreement in F_{LUC} patterns is also reflected in the temporal evolution of annual estimates in the region, with the simulation using the best-guess PFT map resulting in lower F_{LUC} values in the period 1950–1990, but higher values in all other years compared to the simulation based on the default PFT map (Fig. S13).

Similar spatially complex patterns in the altered F_{LUC} estimates under the best-guess PFT map also emerge in other regions. In central parts of Western Africa (IPCC region: WAF), F_{LUC} based on the best-guess PFT map is lower due to the assignment of "C4 natural grasses" in areas where the default PFT map is characterized by "Tropical evergreen forest" (Fig. 6c). In contrast, coastal and northern parts of Western Africa exhibit higher F_{LUC} in the simulation using the best-guess PFT map due to the assignment of forest PFTs in areas dominated by "C4 natural grasses" and "Raingreen shrubs" in the default PFT map. In Central North America (IPCC region: CNA), large areas with forest PFTs in the best-guess PFT map are classified as grass PFTs in the default PFT map, resulting in considerably higher cumulative F_{LUC} in the simulation based on the best-guess PFT map (Fig. 6d).

The spatial patterns in cumulative net F_{LUC} are also reflected in the contributions of individual PFTs (Fig. 5d). Across all four simulations, the PFT "Tropical evergreen forest" consistently exhibits the largest contribution to F_{LUC}, although estimates based on the best-guess PFT map are about 15% lower than those derived from the default PFT map. In contrast, F_{LUC} estimates for "Tropical deciduous forest" are nearly identical across the simulations. Cumulative F_{LUC} is higher for most other forest PFTs in the simulation using the best-guess PFT map. The strongest relative increase is observed for "Temperate evergreen broadleaf forest", where F_{LUC} is nearly five times larger than in the default simulation. Contributions from "Temperate/boreal deciduous broadleaf forest" and "Temperate/boreal evergreen conifers" are also substantially higher, by 60% and 40%, respectively. Differences in shrub and grass PFTs have a mixed influence on their contributions to net F_{LUC}. Similar to "Tropical evergreen forest", F_{LUC} estimates from "Raingreen shrubs" are substantially lower under the best-guess PFT map due to the smaller global extent of this PFT in that map. For "C3 natural grasses", F_{LUC} is slightly higher in simulations using the best-guess PFT map than when based on the default PFT map, whereas the estimates from "C4 natural grasses" remain similar across both simulations despite the pronounced regional differences (Fig. S5). Contributions from "Summergreen shrubs" and "Tundra" are negligible.

https://doi.org/10.5194/egusphere-2026-2682
Preprint. Discussion started: 3 June 2026

4 Discussion

4.1 Novel aspects and strengths of our approach

The global PNV maps developed in this study offer several advances over existing PNV maps. First, we use an expanded training dataset (12 785 data points from 12 404 unique locations), which substantially increases both the size of biome classes and the spatial coverage of sampling points compared to previous studies with a pollen-based PNV mapping approach (e.g., Hengl et al., 2018; Bonannella et al., 2023b) (8 959 data points from 8 057 locations). The preparation of the biome data, including harmonization and aggregation of various regional pollen-based biome reconstructions and removal of duplicate data points, reduces modeling bias and prevents inflated performance metrics. The enhanced compilation of pollen-based biome reconstructions leads to more accurate PNV predictions in certain regions, such as the "Steppe" biome in the southern Patagonian Steppe, which is partly misclassified as forest in previous studies (Hengl et al., 2018; Lindgren et al., 2021; Bonannella et al., 2023b). Second, our approach reduces the subjective bias of traditional expert-based PNV maps (e.g., Olson et al., 2001; Dinerstein et al., 2017; FAO, 2001), as advocated by Champreux et al. (2024), by relating pollen-based biome reconstructions to environmental characteristics for a more objective and data-driven delineation of biome classes. By deliberately selecting environmental predictors that avoid replicating human land-use patterns, our approach prevents the propagation of anthropogenic signals into PNV predictions, which is the central limitation of satellite-based PNV mapping methods (Higgins et al., 2016). Third, deriving a best-guess and two sensitivity PNV maps that return the maximal forest and grass PFT fractions predicted by the ensemble enables the estimation of the uncertainty in the extent of forest and grasses and their impacts on subsequent modeling tasks.

The combined use of two spatial uncertainty metrics (model agreement and model certainty) improves the understanding of ecological and data-driven uncertainties in PNV predictions and helps to identify regions where additional sampling is required. Regions with the highest uncertainty (Fig. 3) predominantly coincide with areas that are underrepresented in the training data and characterized by biome transitions. These transitional zones in the PNV maps often correspond to known ecotones, where gradual ecological shifts between biomes make PNV predictions challenging and uncertain, resulting in lower model agreement. We address such uncertainties by averaging across 30 PFT maps, which returns PFT fractions that partially capture the ecological gradients and account for prediction uncertainty. This is, for instance, illustrated in mountainous regions of Borneo and Sumatra (Fig. S3), where vegetation shifts from lowland tropical rainforest to less dense vegetation with increasing altitude are reflected by decreasing fractions of "Tropical evergreen forests" and increasing fractions of "Temperate evergreen broadleaf forests". However, high model agreement alone does not necessarily imply reliable predictions, as areas that are poorly represented in the training data may show consistent PNV predictions across the 30 PFT maps despite low model certainty (e.g., Bangladesh, southern and western Australia). Areas with low model certainty highlight locations where additional biome data collection is needed to better link the prevalent biomes to environmental conditions and thereby improve the reliability of PNV predictions globally.

https://doi.org/10.5194/egusphere-2026-2682
Preprint. Discussion started: 3 June 2026

The differences between the three PFT maps from this study and the default PFT map of BLUE stem from methodological advances in both the underlying biome maps and the reclassification framework, encompassing improved spatial resolution, updated data sources with longer temporal coverage, and observation-driven PFT allocations. Specifically, our reclassification framework offers a more accurate and spatially explicit representation of ecological gradients compared to the one used to create the default PFT map. By incorporating state-of-the-art datasets, which cover multiple decades and offer a high spatial resolution, our approach reduces the susceptibility of the PFT classifications to short-term climate variability and disturbances. It further minimizes the reliance on uncertain bioclimatic parameter thresholds and predefined allocation fractions during reclassification, which are used in the construction of the default PFT map. The $0.0083°$ spatial resolution of our PNV predictions, and of most datasets used for the reclassification into PFTs, offers an unprecedented level of detail for PFT maps used in bookkeeping models and DGVMs. This resolution is approximately ten times finer than the PNV map of Ramankutty and Foley (1999), which serves as the basis for the default PFT map. The improved spatial accuracy reduces unrealistic PFT borders visible in the default PFT map (Fig. S4), such as artificially straight boundaries and abrupt transitions along grid cells for "Tropical deciduous forest" in southern Brazil or "Raingreen shrubs" on the Iberian Peninsula. Spatial discrepancies in the abiotic surface cover fractions (Fig. S5) between the best-guess PFT map and the default PFT map stem from the updated data source, with Harper et al. (2023) being used instead of Hagemann (2002), but translate into differences in PFT fractions. For instance, the lower "C3 natural grassland" shares in the best-guess PFT map in southern Patagonia result from considerably higher shares of abiotic surface cover in that region. In contrast, the lower areal extent of "Raingreen shrub" in the PFT maps from this study results from improvements in both the underlying biome data and the updated reclassification framework. Shrub PFTs are more abundant in the default PFT map where larger areas allow the occurrence of shrubs and higher allocation fractions (40% or 80%) for shrub PFTs are predefined for the reclassification of mixed vegetation classes into BLUE PFTs. By contrast, our approach utilizes observation-based allocation fractions from Harper et al. (2023) to determine the share of shrub PFTs in a grid cell, which rarely exceeds 40%, leading to a more constrained and spatially variable representation of shrub-dominated systems. In addition to these advancements in the reclassification framework, the higher operational spatial resolution ($0.25°$ in the PFT maps from this study compared to $0.5°$ in the default PFT map) contributes to a more nuanced and observation-driven representation of PNV.

4.2 Differences and uncertainties in F_{LUC} estimates related to PNV

Differences and uncertainties in PNV distribution substantially affect both global and regional F_{LUC} estimates. In particular, cumulative global F_{LUC} for the period 1850–2023 is 16% higher in the simulation using the best-guess PFT map from this study than in the default simulation. This increase is notable because BLUE simulations based on the default PFT map already have the highest global F_{LUC} among the four bookkeeping-model estimates that contribute to the GCB 2024 (Friedlingstein et al., 2025). In contrast, previous studies examining the influence of alternative allocation fractions or land-use change forcing datasets report lower global F_{LUC} estimates relative to the default BLUE configuration (Bastos et al., 2021; Ganzenmüller et al.,

https://doi.org/10.5194/egusphere-2026-2682
Preprint. Discussion started: 3 June 2026

2022).

Transitional biome zones are identified as important areas of uncertainty in the PNV distribution. The influence of this uncertainty on F_{LUC} estimates is quantified by comparing BLUE simulations based on two sensitivity maps maximizing forest and grassland extent. Accordingly, cumulative F_{LUC} for 1850–2023 derived from these sensitivity maps exceeds the default BLUE estimate by 27% and 6%, respectively, illustrating the substantial influence of uncertainty in PNV on F_{LUC} estimates. The resulting range in F_{LUC} estimates is comparable in magnitude to other key sources of model uncertainty previously quantified with BLUE, including uncertainties from land-use change forcing data, model parameterization, and model complexity and setup (Table 2). This indicates that uncertainty in PNV distribution represents a major contributor to the overall uncertainty in F_{LUC} estimates and should be considered alongside these other sources of model uncertainty.

The impact of PNV-related differences and uncertainties on F_{LUC} estimates, particularly in areas where PFT maps differ in the distribution of forest and non-forest PFTs, becomes even more evident on a regional scale. In Southeastern South America, cumulative historical F_{LUC} differences exceeding $100\,\mathrm{tC\,ha^{-1}}$ (Fig. 6) occur where the best-guess PFT map from this study and the default PFT map show opposing forest patterns: in the center of the IPCC region the best-guess PFT map depicts extensive forest that is absent in the default PFT map, whereas the default PFT map assigns higher forest fractions along its northern boundary (Fig. S14). Expert-based PNV maps show similar inconsistencies, with Dinerstein et al. (2017) delineating comparatively lower forest extent, FAO (2012) classifying almost the entire IPCC region as forest, and IBGE (2012) defining broad ecotonal zones with varying transitional states between forests and savannas. The high uncertainties in our underlying PNV predictions, with large areas where multiple biomes have similar probabilities resulting in the low model certainty seen in Fig. 3, contribute to the difficulty of classifying the transitional zones in Southeastern South America. This interpretation is supported by other PNV predictions based on machine learning, such as Bonannella et al. (2023a)(version 2, with biome classes) who predicted substantially smaller forest areas than previous estimates by Hengl (2019) and Bonannella et al. (2023a)(version 2, with IUCN classes), despite using the same biome training data.

Other IPCC regions with pronounced impacts of PNV-related uncertainties on F_{LUC} estimates are Western Africa and Central North America. In Western Africa, estimates based on the best-guess PFT map are probably overestimated in the northern part of the region due to forest artifacts introduced by the reclassification scheme (Fig. S15). Vegetation patterns in these drylands are difficult to assess, with satellite-based maps and DGVM simulations revealing strong disagreement on the spatial distribution of trees and aboveground carbon densities (Tucker et al., 2023). Along the coastline, the forest distribution in the best-guess PFT map aligns well with Dinerstein et al. (2017) but extends further north along the western coast in agreement with the higher tropical tree cover fractions reported by Brandt et al. (2023). Inland, high forest PFT fractions along 10°N in the default PFT map are not present in other PNV maps apart from FAO (2012), which classifies nearly the entire IPCC region as forest due to the absence of a distinct savanna category. In Central North America, higher F_{LUC} estimates under the best-guess PFT map are attributed to the forest-grassland boundary being located further west compared to the default PFT

https://doi.org/10.5194/egusphere-2026-2682
Preprint. Discussion started: 3 June 2026

Table 2. Factors influencing estimates of the global net CO_2 flux from land use and land-use change (F_{LUC}) quantified with the bookkeeping model BLUE (Hansis et al., 2015). Reported values show the relative change in F_{LUC} estimates for each factor, expressed as percentage of the respective default simulation used in each study. The comparison expands on Tab. 1 of Pongratz et al. (2021) but is limited to studies using the bookkeeping model BLUE. Differences in simulated time periods, land-use change (LUC) forcings, and the inconsistent treatment of emissions from peat burning and peat drainage affect the comparability across studies.

Uncertainty category	**Quantified uncertainty**	
This study	**Cumulative F_{LUC} (1850–2023)**	
PNV distribution	16%	Increase using the best-guess PFT map (PFT_{ML})
PNV distribution	21%	Difference attributed to maximum biome value ranges (spread between $PFT_{MLforest}$ and $PFT_{MLgrass}$)
Ganzenmüller et al. (2022)	**Mean annual F_{LUC} (1960–2019)**	
LUC dataset	35%	Decrease under the LUC dataset HILDA+[a] compared to LUH2
Spatial resolution	4%	Difference attributed to the spatial resolution (LUC forcing with HILDA+[a] at 0.25° and 0.01°)
Bastos et al. (2021)	**Cumulative F_{LUC} (1850–2015)[b]**	
Model complexity	14%	Increase attributed to the implementation of gross land cover transitions
Parameterization	25%	Decrease using the carbon densities of HN2017[c]
Parameterization	34%	Decrease using the allocation fractions of HN2017[c]
Parameterization	3%	Increase using the decay times of HN2017[c]
Hartung et al. (2021)	**Cumulative F_{LUC} (1850–2015)**	
Model setup	15%	Difference attributed to the initialization year
Model complexity	13%	Difference attributed to the implementation of land cover transitions (gross vs. net transitions)
LUC dataset	22%	Difference attributed to the LUC dataset
Model complexity	28%	Decrease from neglecting wood harvest
Dorgeist et al. (2024)	**F_{LUC} (1850–2021)**	
Parameterization	11%	Increase under transient carbon densities (carbon densities responding to changes in environmental conditions)

[a] HILDA+ refers to the land-use change dataset HIstoric Land Dynamics Assessment + (Winkler et al., 2021).
[b] Percentage difference compared to the BLUE simulation with net land cover transitions. The default setup of BLUE uses gross land cover transitions.
[c] HN2017 refers to the bookkeeping model of Houghton and Nassikas (2017).

https://doi.org/10.5194/egusphere-2026-2682
Preprint. Discussion started: 3 June 2026

map (Fig. S16), which is also observed in other PNV maps based on machine learning (Bonannella et al., 2023a; Hengl, 2019). This westward expansion of forest PFTs at the expense of grass PFTs could be explained by the absence of fire and grazing effects in our training data, which are relevant drivers of natural vegetation cover (Bastin et al., 2025) and constrain tree establishment in the eastern Great Plains despite suitable climatic conditions (Sankaran et al., 2004; Anderson, 2006; CEC, 1997). The discrepancies across all three IPCC regions (Southeastern South America, Western Africa, and Central North America) further illustrate how PNV maps, independent of their classification approach, struggle to represent vegetation through discrete classes in transitional landscapes that are ecologically complex and characterized by mixed physiognomies.

Overall, the comparison of different PNV maps reveals major inconsistencies across regions, which arise from different mapping approaches, the difficulty of representing complex vegetation mosaics through discrete classes, and extensive anthropogenic land-use change resulting in a lack of continuous ground-truth data required to assess which PNV map is more realistic. The suitability of regional vegetation maps to represent PNV is limited, as they are partly (U.S. EPA, 2010), largely (IBGE, 2012), or entirely (Brandt et al., 2023) derived from satellite observations. In contrast, global PNV maps, particularly the global ecological zones for FAO forest reporting (FAO, 2012), lack the ecological and spatial resolution necessary to obtain detailed and spatially explicit F_{LUC} estimates and fail to adequately represent mixed vegetation classes, such as savannas, which encompass varying proportions of trees, shrubs, and grasses.

4.3 Limitations

Although the PFT maps developed in this study advance data-driven estimates of global PNV, our approach has several limitations. First, the training dataset is imbalanced across biomes and spatially biased. The samples disproportionately represent productive ecosystems and temperate regions (Fig. 2a) and spatial autocorrelation among clustered samples likely results in an overestimated model performance (Roberts et al., 2017; Schratz et al., 2019). Additionally, the large amount of pollen produced by woody taxa can mask vegetation producing less pollen (Binney et al., 2017), leading to overrepresentation of forests in pollen-based biome reconstructions (approximately 65% of the 12 785 samples are forest biomes). Forest extent is thus likely overestimated in the global PNV predictions, particularly if the real biome of a location is not represented in the input data or environmental conditions lie outside those covered by the predictor space of the training data. Second, the discrete structure of the random forest classifiers, which assign only one biome class per grid cell, prevents the representation of gradual biome transitions and mosaics of vegetation types that characterize many landscapes on a sub-grid scale. We address this limitation by using a high spatial resolution (0.0083°), the ensemble mean of 30 PNV maps, and the fractional allocation of mixed biome classes to individual PFTs, which allows our PFT maps to depict transitional ecozones more effectively than alternative PNV mapping approaches (Figs. S14–S16). Third, the use of the satellite-based CCI PFT data (Harper et al., 2023) for allocating PNV predictions to BLUE PFTs potentially introduces anthropogenic land-use patterns into the PFT maps of this study. Since the CCI PFT dataset only defines two anthropogenic PFTs (“managed grasses”, which include croplands, and “built-up area”), all other forms of anthropogenic land-use elements, such as planted forests, plantations, or large-scale mining operations, may be partly integrated into the PFT maps. However, apart from anthropogenic changes to the abiotic surface cover fraction, this

https://doi.org/10.5194/egusphere-2026-2682
Preprint. Discussion started: 3 June 2026

issue only affects the allocation of mixed biome classes and cannot be avoided, as the plant functional traits of such areas under PNV are unknown and cannot be determined. Moreover, the assumption of proportional replacement, in which it is assumed that changes in land use replace vegetation types proportionally, simplifies actual dynamics of land use and may affect the estimates of F_{LUC}. For example, Reick et al. (2013) show that preferential establishment of pastures on grasslands leads to lower deforestation than under proportional allocation. Lastly, insufficient ground-truth data for PNV in many regions and difficulties in comparing PNV maps due to different conceptual approaches, classification criteria, and vegetation classes limit the independent evaluation of our PNV and PFT maps (Conradi et al., 2020).

Beyond these general constraints in the construction of our PNV and PFT maps, their implementation in BLUE introduces limitations specific to the modeled F_{LUC} estimates. First, our approach to constructing PNV maps does not account for transient effects on the spatial distribution of PFTs (e.g., due to climate change or tipping points), as we rely on present-day vegetation observations and environmental conditions to generate PNV maps, a procedure in line with the definition of potential natural vegetation (Tüxen, 1956). It is an ongoing discussion whether environmental changes that influence F_{LUC} estimates (e.g., by altering standing carbon stocks or regrowth behavior) should or should not be considered in estimates of carbon emissions and removals of land-use change (Houghton, 2013; Pongratz et al., 2014; Dorgeist et al., 2024; Obermeier et al., 2021). Most recent estimates of the Global Carbon Budget have adopted the approach of using transient carbon densities, which respond to environmental changes, instead of fixed carbon densities based on present-day observations (Friedlingstein et al., 2026). Following the logic of reflecting transient carbon densities, natural changes to the PFT distribution should also be considered in models simulating F_{LUC}. However, it is typically assumed that the dynamics in the natural biogeographic distribution of vegetation occur slowly due to slow plant migration rates (Svenning and Sandel, 2013) and limiting factors such as slow soil formation and nutrient limitations in cold regions, which become favorable for vegetation growth under global warming (Huang et al., 2017). As a result, these dynamics are less relevant for estimates of the 20th century carbon cycle but have increased importance for multi-century studies of land-use impacts on climate (Pongratz et al., 2009; Stocker et al., 2011).

Furthermore, the use of PNV maps in current bookkeeping models ignores that a considerable share of global forest area consists of planted forests and forests influenced by other human management (Lesiv et al., 2022; Schulze et al., 2019; Winkler et al., 2021), which can result in differences between observed PFTs and those represented in PNV maps. While bookkeeping models typically account for wood harvesting, they do not include other management activities such as tree species selection. The resulting mismatches affect F_{LUC} estimates, as parameter values for carbon densities, allocation fractions, and residence times refer to potential PFTs instead of actual PFTs (e.g., using mixed broadleaf forests that would grow naturally in a certain location instead of the actual spruce monoculture planted by humans). Consequently, simulated F_{LUC} is overestimated if the assigned PFT has higher carbon densities than the actual vegetation and underestimated if the opposite is true. For example, we estimate higher F_{LUC} emissions during 2000–2023 in parts of south-western China under the best-guess PFT map than under the default PFT map of BLUE. This difference stems from the assignment of the PFT "Temperate evergreen broadleaf forests" in the best-guess PFT map, which has higher carbon densities than the PFT "Temperate/boreal evergreen conifers" assigned in

https://doi.org/10.5194/egusphere-2026-2682
Preprint. Discussion started: 3 June 2026

the default PFT map and thus results in higher F_{LUC} estimates upon deforestation and wood harvest. Despite the relevance of this mismatch, the PNV of this region cannot be determined with certainty due to the long history of anthropogenic land-use activities. Here, our results as well as Dinerstein et al. (2017), Zhang et al. (2024), or Haxeltine and Prentice (1996) indicate evergreen broadleaf forests, whereas Ramankutty and Foley (1999), using satellite observation, indicate needleleaf forests due to the substantial fraction of planted forests dominated by coniferous trees (Yu et al., 2022; Abbasi et al., 2023).

4.4 Relevance for carbon cycle research and climate mitigation

Quantifying the previously unexplored influence of PNV on F_{LUC} estimates has important implications for carbon cycle research and climate change mitigation. The level of uncertainty in F_{LUC} associated with the global PNV distribution is comparable to that from other key sources, such as land-use change forcing and model parameterization. Providing enhanced PFT maps as input to F_{LUC} models, including specifically developed sensitivity maps, therefore represents an important step towards more robust estimates of global and regional F_{LUC}. The temporal evolution of the component fluxes indicates that F_{LUC} estimates remain sensitive to differences in underlying PNV distributions in both historical periods and recent years. At regional scales, pronounced differences between BLUE simulations using different PFT maps, particularly in transitional zones between biomes, highlight the importance of empirically grounded, high-resolution PNV reconstructions for capturing the spatial heterogeneity of F_{LUC} linked to small-scale vegetation characteristics. The substantially larger forest PFT area (+20%) and smaller shrub PFT area (–73%) in the best-guess PFT map relative to the default PFT map of BLUE suggest an increased potential for carbon dioxide removal (CDR) due to the larger area suitable for afforestation and reforestation. Overall, these results highlight the value of refined PNV representation in models and of explicitly accounting for PNV-related uncertainties when quantifying F_{LUC}. The remaining uncertainties in the mapped PNV distributions, particularly in transitional zones and sparsely sampled regions, emphasize the need for improved sample coverage to enhance the reliability of future PNV mapping approaches. A more comprehensive sample coverage could further enable the inclusion of additional biome classes, leading to a more nuanced representation of heterogeneous landscapes in models quantifying F_{LUC}. Ultimately, the data-driven framework presented here provides a foundation for more reliable F_{LUC} estimates and reinforces the central role of accurate PNV maps in compiling robust carbon budgets and developing effective climate change mitigation strategies.

https://doi.org/10.5194/egusphere-2026-2682
Preprint. Discussion started: 3 June 2026

595 *Code and data availability.* Data and code are available upon request from the corresponding author and will be made available at the Zenodo repository.

Author contributions. Conceptualization, A.I.R.J., J.P., R.G.; methodology, A.I.R.J., R.G.; investigation, A.I.R.J.; visualization, A.I.R.J.; writing – original draft, A.I.R.J., W.A.O., C.S., A.A., R.G.; writing – review & editing, A.I.R.J., W.A.O., C.S., A.A., J.P., R.G..

Competing interests. The authors declare no competing interests.

600 *Acknowledgements.* We thank Henri Funk and Yichen Han from the Statistical Consulting Unit (StaBLab) at the LMU Munich for their guidance during the initial development of the ML approach. A.A. acknowledges support from the German Federal Ministry of Education and Research (Grant No. 01LS2301A, project CDRatlas). R.G. acknowledges support from the European Commission through the Horizon 2020 Framework Programme (VERIFY, grant no. 776810). This work used resources of the Deutsches Klimarechenzentrum (DKRZ) granted by its Scientific Steering Committee (WLA) under project ID bm0891.

https://doi.org/10.5194/egusphere-2026-2682
Preprint. Discussion started: 3 June 2026

References

Abbasi, A. O., Tang, X., Harris, N. L., Goldman, E. D., Gamarra, J. G. P., Herold, M., Kim, H. S., Luo, W., Silva, C. A., Tchebakova, N. M., Mitra, A., Finegold, Y., Jahanshahi, M. R., Alvarez, C. I., Kim, T. K., Ryu, D., and Liang, J.: Spatial Database of Planted Forests in East Asia, Sci. Data, 10, 480, https://doi.org/10.1038/s41597-023-02383-w, 2023.

Anderson, R. C.: Evolution and Origin of the Central Grassland of North America: Climate, Fire, and Mammalian Grazers 1, J. Torrey Bot. Soc., 133, 626–647, https://doi.org/10.3159/1095-5674(2006)133[626:EAOOTC]2.0.CO;2, 2006.

Arneth, A., Sitch, S., Pongratz, J., Stocker, B. D., Ciais, P., Poulter, B., Bayer, A. D., Bondeau, A., Calle, L., Chini, L. P., Gasser, T., Fader, M., Friedlingstein, P., Kato, E., Li, W., Lindeskog, M., Nabel, J. E. M. S., Pugh, T. A. M., Robertson, E., Viovy, N., Yue, C., and Zaehle, S.: Historical Carbon Dioxide Emissions Caused by Land-Use Changes Are Possibly Larger than Assumed, Nat. Geosci., 10, 79–84, https://doi.org/10.1038/ngeo2882, 2017.

Bastin, J.-F., Latte, N., Bogaert, J., Garcia, C. A., Berzaghi, F., Maestre, F. T., Svenning, J.-C., Assede, E., Barima, S., Besisa, T., Bouchoms, S., Crowther, T. W., de Haulleville, T., de Lame, H., Depoortere, P., Dufrêne, M., van Hoek Dijke, A. J., Lhoest, S., Mahy, G., Messier, C., Mollicone, D., Ramalason, F. N., Peaucelle, M., Plumacker, A., Quétier, F., Rakotondrasoa, O., Sambieni, K. R., Sparrow, B., Tarelkin, Y., Sikuzani, Y. U., Vander Linden, A., and Lejeune, P.: Global Alternatives of Natural Vegetation Cover, Nat. Commun., 16, 6484, https://doi.org/10.1038/s41467-025-61520-8, 2025.

Bastos, A., Hartung, K., Nützel, T. B., Nabel, J. E. M. S., Houghton, R. A., and Pongratz, J.: Comparison of Uncertainties in Land-Use Change Fluxes from Bookkeeping Model Parameterisation, Earth Syst. Dyn., 12, 745–762, https://doi.org/10.5194/esd-12-745-2021, 2021.

Beigaitė, R., Tang, H., Bryn, A., Skarpaas, O., Stordal, F., Bjerke, J. W., and Žliobaitė, I.: Identifying Climate Thresholds for Dominant Natural Vegetation Types at the Global Scale Using Machine Learning: Average Climate versus Extremes, Glob. Change Biol., 28, 3557–3579, https://doi.org/10.1111/gcb.16110, 2022a.

Beigaitė, R., Read, J., and Žliobaitė, I.: Multi-Output Regression with Structurally Incomplete Target Labels: A Case Study of Modelling Global Vegetation Cover, Ecol. Inform., 72, 101 849, https://doi.org/10.1016/j.ecoinf.2022.101849, 2022b.

Bekkar, M., Djemaa, H. K., and Alitouche, T. A.: Evaluation Measures for Models Assessment over Imbalanced Data Sets, J. Inf. Eng. Appl., 3, 80–97, 2013.

Binney, H., Edwards, M., Macias-Fauria, M., Lozhkin, A., Anderson, P., Kaplan, J. O., Andreev, A., Bezrukova, E., Blyakharchuk, T., Jankovska, V., Khazina, I., Krivonogov, S., Kremenetski, K., Nield, J., Novenko, E., Ryabogina, N., Solovieva, N., Willis, K., and Zernitskaya, V.: Vegetation of Eurasia from the Last Glacial Maximum to Present: Key Biogeographic Patterns, Quat. Sci. Rev., 157, 80–97, https://doi.org/10.1016/j.quascirev.2016.11.022, 2017.

Bischl, B., Binder, M., Lang, M., Pielok, T., Richter, J., Coors, S., Thomas, J., Ullmann, T., Becker, M., Boulesteix, A.-L., Deng, D., and Lindauer, M.: Hyperparameter Optimization: Foundations, Algorithms, Best Practices, and Open Challenges, WIREs Data Min. Knowl. Discov., 13, e1484, https://doi.org/10.1002/widm.1484, 2023.

Bonannella, C., Hengl, T., Heisig, J., Parente, L., Wright, M. N., Herold, M., and de Bruin, S.: Forest Tree Species Distribution for Europe 2000-2020: Mapping Potential and Realized Distributions Using Spatiotemporal Machine Learning, PeerJ, 10, e13 728, https://doi.org/10.7717/peerj.13728, 2022.

Bonannella, C., Hengl, T., Leal Parente, L., and de Bruin, S.: Current and Future Global Distribution of Potential Biomes under Climate Change Scenarios. (Version 2), Zenodo [data set], https://doi.org/10.5281/zenodo.7822868, 2023a.

https://doi.org/10.5194/egusphere-2026-2682
Preprint. Discussion started: 3 June 2026

Bonannella, C., Hengl, T., Parente, L., and de Bruin, S.: Biomes of the World under Climate Change Scenarios: Increasing Aridity and Higher Temperatures Lead to Significant Shifts in Natural Vegetation, PeerJ, 11, e15 593, https://doi.org/10.7717/peerj.15593, 2023b.

Brandt, J., Ertel, J., Spore, J., and Stolle, F.: Wall-to-Wall Mapping of Tree Extent in the Tropics with Sentinel-1 and Sentinel-2, Remote Sens. Environ., 292, 113 574, https://doi.org/10.1016/j.rse.2023.113574, 2023.

CEC: Ecological Regions of North America – toward a Common Perspective, Commission for Environmental Cooperation, Montreal, ISBN 2-922305-18-X, 1997.

Champreux, A., Saltré, F., Traylor, W., Hickler, T., and Bradshaw, C. J. A.: How to Map Biomes: Quantitative Comparison and Review of Biome–Mapping Methods, Ecol. Monogr., 94, e1615, https://doi.org/10.1002/ecm.1615, 2024.

Chiarucci, A., Araújo, M. B., Decocq, G., Beierkuhnlein, C., and Fernández-Palacios, J. M.: The Concept of Potential Natural Vegetation: An Epitaph?, J. Veg. Sci., 21, 1172–1178, https://doi.org/10.1111/j.1654-1103.2010.01218.x, 2010.

Chicco, D. and Jurman, G.: The Advantages of the Matthews Correlation Coefficient (MCC) over F1 Score and Accuracy in Binary Classification Evaluation, BMC Genomics, 21, 6, https://doi.org/10.1186/s12864-019-6413-7, 2020.

Chini, L., Hurtt, G., Sahajpal, R., Frolking, S., Klein Goldewijk, K., Sitch, S., Ganzenmüller, R., Ma, L., Ott, L., Pongratz, J., and Poulter, B.: Land-Use Harmonization Datasets for Annual Global Carbon Budgets, Earth Syst. Sci. Data, 13, 4175–4189, https://doi.org/10.5194/essd-13-4175-2021, 2021.

Conradi, T., Slingsby, J. A., Midgley, G. F., Nottebrock, H., Schweiger, A. H., and Higgins, S. I.: An Operational Definition of the Biome for Global Change Research, New Phytol., 227, 1294–1306, https://doi.org/10.1111/nph.16580, 2020.

Copernicus Climate Change Service: Land Cover Classification Gridded Maps from 1992 to Present Derived from Satellite Observations, ECMWF [data set], https://doi.org/10.24381/cds.006f2c9a, 2019.

Dallmeyer, A., Claussen, M., and Brovkin, V.: Harmonising Plant Functional Type Distributions for Evaluating Earth System Models, Clim. Past, 15, 335–366, https://doi.org/10.5194/cp-15-335-2019, 2019.

Dietze, M. C.: Prediction in Ecology: A First-Principles Framework, Ecol. Appl., 27, 2048–2060, https://doi.org/10.1002/eap.1589, 2017.

Dinerstein, E., Olson, D., Joshi, A., Vynne, C., Burgess, N. D., Wikramanayake, E., Hahn, N., Palminteri, S., Hedao, P., Noss, R., Hansen, M., Locke, H., Ellis, E. C., Jones, B., Barber, C. V., Hayes, R., Kormos, C., Martin, V., Crist, E., Sechrest, W., Price, L., Baillie, J. E. M., Weeden, D., Suckling, K., Davis, C., Sizer, N., Moore, R., Thau, D., Birch, T., Potapov, P., Turubanova, S., Tyukavina, A., de Souza, N., Pintea, L., Brito, J. C., Llewellyn, O. A., Miller, A. G., Patzelt, A., Ghazanfar, S. A., Timberlake, J., Klöser, H., Shennan-Farpón, Y., Kindt, R., Lillesø, J.-P. B., van Breugel, P., Graudal, L., Voge, M., Al-Shammari, K. F., and Saleem, M.: An Ecoregion-Based Approach to Protecting Half the Terrestrial Realm, BioScience, 67, 534–545, https://doi.org/10.1093/biosci/bix014, 2017.

Dorgeist, L., Schwingshackl, C., Bultan, S., and Pongratz, J.: A Consistent Budgeting of Terrestrial Carbon Fluxes, Nat. Commun., 15, 7426, https://doi.org/10.1038/s41467-024-51126-x, 2024.

Elsen, P. R., Saxon, E. C., Simmons, B. A., Ward, M., Williams, B. A., Grantham, H. S., Kark, S., Levin, N., Perez-Hammerle, K.-V., Reside, A. E., and Watson, J. E. M.: Accelerated Shifts in Terrestrial Life Zones under Rapid Climate Change, Glob. Change Biol., 28, 918–935, https://doi.org/10.1111/gcb.15962, 2022.

FAO: Global Ecological Zoning for the Global Forest Resources Assessment 2000, Food and Agriculture Organization of the United Nations, Rome, 2001.

FAO: Global Ecological Zones for FAO Forest Reporting: 2010 Update, Food and Agriculture Organization of the United Nations, Rome, 2012.

https://doi.org/10.5194/egusphere-2026-2682
Preprint. Discussion started: 3 June 2026

Fischer, J.-C., Walentowitz, A., and Beierkuhnlein, C.: The Biome Inventory – Standardizing Global Biogeographical Land Units, Glob. Ecol. Biogeogr., 31, 2172–2183, https://doi.org/10.1111/geb.13574, 2022.

Flantua, S. G., Hooghiemstra, H., Grimm, E. C., Behling, H., Bush, M. B., González-Arango, C., Gosling, W. D., Ledru, M.-P., Lozano-García, S., Maldonado, A., Prieto, A. R., Rull, V., and van Boxel, J. H.: Updated Site Compilation of the Latin American Pollen Database, Rev. Palaeobot. Palynol., 223, 104–115, https://doi.org/10.1016/j.revpalbo.2015.09.008, 2015.

Friedl, M. A., Sulla-Menashe, D., Tan, B., Schneider, A., Ramankutty, N., Sibley, A., and Huang, X.: MODIS Collection 5 Global Land Cover: Algorithm Refinements and Characterization of New Datasets, Remote Sens. Environ., 114, 168–182, https://doi.org/10.1016/j.rse.2009.08.016, 2010.

Friedlingstein, P., O'Sullivan, M., Jones, M. W., Andrew, R. M., Hauck, J., Landschützer, P., Le Quéré, C., Li, H., Luijkx, I. T., Olsen, A., Peters, G. P., Peters, W., Pongratz, J., Schwingshackl, C., Sitch, S., Canadell, J. G., Ciais, P., Jackson, R. B., Alin, S. R., Arneth, A., Arora, V., Bates, N. R., Becker, M., Bellouin, N., Berghoff, C. F., Bittig, H. C., Bopp, L., Cadule, P., Campbell, K., Chamberlain, M. A., Chandra, N., Chevallier, F., Chini, L. P., Colligan, T., Decayeux, J., Djeutchouang, L. M., Dou, X., Duran Rojas, C., Enyo, K., Evans, W., Fay, A. R., Feely, R. A., Ford, D. J., Foster, A., Gasser, T., Gehlen, M., Gkritzalis, T., Grassi, G., Gregor, L., Gruber, N., Gürses, Ö., Harris, I., Hefner, M., Heinke, J., Hurtt, G. C., Iida, Y., Ilyina, T., Jacobson, A. R., Jain, A. K., Jarníková, T., Jersild, A., Jiang, F., Jin, Z., Kato, E., Keeling, R. F., Klein Goldewijk, K., Knauer, J., Korsbakken, J. I., Lan, X., Lauvset, S. K., Lefèvre, N., Liu, Z., Liu, J., Ma, L., Maksyutov, S., Marland, G., Mayot, N., McGuire, P. C., Metzl, N., Monacci, N. M., Morgan, E. J., Nakaoka, S.-I., Neill, C., Niwa, Y., Nützel, T., Olivier, L., Ono, T., Palmer, P. I., Pierrot, D., Qin, Z., Resplandy, L., Roobaert, A., Rosan, T. M., Rödenbeck, C., Schwinger, J., Smallman, T. L., Smith, S. M., Sospedra-Alfonso, R., Steinhoff, T., Sun, Q., Sutton, A. J., Séférian, R., Takao, S., Tatebe, H., Tian, H., Tilbrook, B., Torres, O., Tourigny, E., Tsujino, H., Tubiello, F., van der Werf, G., Wanninkhof, R., Wang, X., Yang, D., Yang, X., Yu, Z., Yuan, W., Yue, X., Zaehle, S., Zeng, N., and Zeng, J.: Global Carbon Budget 2024, Earth Syst. Sci. Data, 17, 965–1039, https://doi.org/10.5194/essd-17-965-2025, 2025.

Friedlingstein, P., Le Quéré, C., O'Sullivan, M., Hauck, J., Landschützer, P., Luijkx, I. T., Li, H., van der Woude, A., Schwingshackl, C., Pongratz, J., Regnier, P., Andrew, R. M., Bakker, D. C. E., Canadell, J. G., Ciais, P., Gasser, T., Jones, M. W., Lan, X., Morgan, E., Olsen, A., Peters, G. P., Peters, W., Sitch, S., and Tian, H.: Emerging Climate Impact on Carbon Sinks in a Consolidated Carbon Budget, Nature, 649, 98–103, https://doi.org/10.1038/s41586-025-09802-5, 2026.

Ganzenmüller, R., Bultan, S., Winkler, K., Fuchs, R., Zabel, F., and Pongratz, J.: Land-Use Change Emissions Based on High-Resolution Activity Data Substantially Lower than Previously Estimated, Environ. Res. Lett., 17, 064 050, https://doi.org/10.1088/1748-9326/ac70d8, 2022.

Ganzenmüller, R., Obermeier, W. A., Bultan, S., Spawn-Lee, S. A., Zabel, F., and Pongratz, J.: Humans Have Depleted Global Terrestrial Carbon Stocks by a Quarter, One Earth, 8, 101 392, https://doi.org/10.1016/j.oneear.2025.101392, 2025.

Gasser, T., Crepin, L., Quilcaille, Y., Houghton, R. A., Ciais, P., and Obersteiner, M.: Historical CO2 Emissions from Land Use and Land Cover Change and Their Uncertainty, Biogeosciences, 17, 4075–4101, https://doi.org/10.5194/bg-17-4075-2020, 2020.

Griffith, D. M., Anderson, T. M., Osborne, C. P., Strömberg, C. A. E., Forrestel, E. J., and Still, C. J.: Biogeographically Distinct Controls on C 3 and C 4 Grass Distributions: Merging Community and Physiological Ecology, Glob. Ecol. Biogeogr., 24, 304–313, https://doi.org/10.1111/geb.12265, 2015.

Hagemann, S.: An Improved Land Surface Parameter Dataset for Global and Regional Climate Models, Tech. Rep. 336, Max-Planck-Institut für Meteorologie, Hamburg, Germany, https://doi.org/10.17617/2.2344576, 2002.

https://doi.org/10.5194/egusphere-2026-2682
Preprint. Discussion started: 3 June 2026

Hansis, E., Davis, S. J., and Pongratz, J.: Relevance of Methodological Choices for Accounting of Land Use Change Carbon Fluxes, Glob. Biogeochem. Cycles, 29, 1230–1246, https://doi.org/10.1002/2014GB004997, 2015.

Harper, A. B., Powell, T., Cox, P. M., House, J., Huntingford, C., Lenton, T. M., Sitch, S., Burke, E., Chadburn, S. E., Collins, W. J., Comyn-Platt, E., Daioglou, V., Doelman, J. C., Hayman, G., Robertson, E., van Vuuren, D., Wiltshire, A., Webber, C. P., Bastos, A., Boysen, L., Ciais, P., Devaraju, N., Jain, A. K., Krause, A., Poulter, B., and Shu, S.: Land-Use Emissions Play a Critical Role in Land-Based Mitigation for Paris Climate Targets, Nat. Commun., 9, 2938, https://doi.org/10.1038/s41467-018-05340-z, 2018.

Harper, K. L., Lamarche, C., Hartley, A., Peylin, P., Ottlé, C., Bastrikov, V., San Martín, R., Bohnenstengel, S. I., Kirches, G., Boettcher, M., Shevchuk, R., Brockmann, C., and Defourny, P.: A 29-Year Time Series of Annual 300 m Resolution Plant-Functional-Type Maps for Climate Models, Earth Syst. Sci. Data, 15, 1465–1499, https://doi.org/10.5194/essd-15-1465-2023, 2023.

Harrison, S.: BIOME 6000 DB Classified Plotfile Version 1, University of Reading [data set], https://doi.org/10.17864/1947.99, 2017.

Hartung, K., Bastos, A., Chini, L., Ganzenmüller, R., Havermann, F., Hurtt, G. C., Loughran, T., Nabel, J. E. M. S., Nützel, T., Obermeier, W. A., and Pongratz, J.: Bookkeeping Estimates of the Net Land-Use Change Flux – a Sensitivity Study with the CMIP6 Land-Use Dataset, Earth Syst. Dyn., 12, 763–782, https://doi.org/10.5194/esd-12-763-2021, 2021.

Haxeltine, A. and Prentice, I. C.: BIOME3: An Equilibrium Terrestrial Biosphere Model Based on Ecophysiological Constraints, Resource Availability, and Competition among Plant Functional Types, Glob. Biogeochem. Cycles, 10, 693–709, https://doi.org/10.1029/96GB02344, 1996.

Hengl, T.: Potential Distribution of Biomes (Potential Natural Vegetation) at 250 m Spatial Resolution. Version v0.2, Zenodo [data set], https://doi.org/10.5281/zenodo.3526620, 2019.

Hengl, T., Walsh, M. G., Sanderman, J., Wheeler, I., Harrison, S. P., and Prentice, I. C.: Global Mapping of Potential Natural Vegetation: An Assessment of Machine Learning Algorithms for Estimating Land Potential, PeerJ, 6, e5457, https://doi.org/10.7717/peerj.5457, 2018.

Higgins, S. I., Buitenwerf, R., and Moncrieff, G. R.: Defining Functional Biomes and Monitoring Their Change Globally, Glob. Change Biol., 22, 3583–3593, https://doi.org/10.1111/gcb.13367, 2016.

Holdridge, L. R.: Life Zone Ecology, Tropical Science Center, San Jose, 1967.

Houghton, R. A.: Keeping Management Effects Separate from Environmental Effects in Terrestrial Carbon Accounting, Glob. Change Biol., 19, 2609–2612, https://doi.org/10.1111/gcb.12233, 2013.

Houghton, R. A. and Castanho, A.: Annual Emissions of Carbon from Land Use, Land-Use Change, and Forestry from 1850 to 2020, Earth Syst. Sci. Data, 15, 2025–2054, https://doi.org/10.5194/essd-15-2025-2023, 2023.

Houghton, R. A. and Nassikas, A. A.: Global and Regional Fluxes of Carbon from Land Use and Land Cover Change 1850–2015, Glob. Biogeochem. Cycles, 31, 456–472, https://doi.org/10.1002/2016GB005546, 2017.

Huang, M., Piao, S., Janssens, I. A., Zhu, Z., Wang, T., Wu, D., Ciais, P., Myneni, R. B., Peaucelle, M., Peng, S., Yang, H., and Peñuelas, J.: Velocity of Change in Vegetation Productivity over Northern High Latitudes, Nat. Ecol. Evol., 1, 1649–1654, https://doi.org/10.1038/s41559-017-0328-y, 2017.

IBGE: Manual Técnico Da Vegetação Brasileira., vol. número 1 of *Manuais Técnicos Em Geociências*, Instituto Brasileiro de Geografia e Estatística (IBGE), Rio de Janeiro, 2ª edição revista e ampliada edn., ISBN 978-85-240-4272-0, 2012.

IPCC: Climate Change and Land: An IPCC Special Report on Climate Change, Desertification, Land Degradation, Sustainable Land Management, Food Security, and Greenhouse Gas Fluxes in Terrestrial Ecosystems, Cambridge, UK and New York, NY, USA, https://doi.org/10.1017/9781009157988, 2019.

https://doi.org/10.5194/egusphere-2026-2682
Preprint. Discussion started: 3 June 2026

Jurman, G., Riccadonna, S., and Furlanello, C.: A Comparison of MCC and CEN Error Measures in Multi-Class Prediction, PLOS ONE, 7, e41 882, https://doi.org/10.1371/journal.pone.0041882, 2012.

Kaplan, J. O., Bigelow, N. H., Prentice, I. C., Harrison, S. P., Bartlein, P. J., Christensen, T. R., Cramer, W., Matveyeva, N. V., McGuire, A. D., Murray, D. F., Razzhivin, V. Y., Smith, B., Walker, D. A., Anderson, P. M., Andreev, A. A., Brubaker, L. B., Edwards, M. E., and Lozhkin, A. V.: Climate Change and Arctic Ecosystems: 2. Modeling, Paleodata–Model Comparisons, and Future Projections, J. Geophys. Res. Atmospheres, 108, https://doi.org/10.1029/2002JD002559, 2003.

Kohavi, R.: A Study of Cross-Validation and Bootstrap for Accuracy Estimation and Model Selection, in: Proceedings of the 14th International Joint Conference on Artificial Intelligence - Volume 2, IJCAI'95, pp. 1137–1143, Morgan Kaufmann Publishers Inc, Montreal, Quebec, Canada, ISBN 1-55860-363-8, 1995.

Lesiv, M., Schepaschenko, D., Buchhorn, M., See, L., Dürauer, M., Georgieva, I., Jung, M., Hofhansl, F., Schulze, K., Bilous, A., Blyshchyk, V., Mukhortova, L., Brenes, C. L. M., Krivobokov, L., Ntie, S., Tsogt, K., Pietsch, S. A., Tikhonova, E., Kim, M., Di Fulvio, F., Su, Y.-F., Zadorozhniuk, R., Sirbu, F. S., Panging, K., Bilous, S., Kovalevskii, S. B., Kraxner, F., Rabia, A. H., Vasylyshyn, R., Ahmed, R., Diachuk, P., Kovalevskyi, S. S., Bungnamei, K., Bordoloi, K., Churilov, A., Vasylyshyn, O., Sahariah, D., Tertyshnyi, A. P., Saikia, A., Malek, Ž., Singha, K., Feshchenko, R., Prestele, R., Akhtar, I. U. H., Sharma, K., Domashovets, G., Spawn-Lee, S. A., Blyshchyk, O., Slyva, O., Ilkiv, M., Melnyk, O., Sliusarchuk, V., Karpuk, A., Terentiev, A., Bilous, V., Blyshchyk, K., Bilous, M., Bogovyk, N., Blyshchyk, I., Bartalev, S., Yatskov, M., Smets, B., Visconti, P., Mccallum, I., Obersteiner, M., and Fritz, S.: Global Forest Management Data for 2015 at a 100 m Resolution, Sci. Data, 9, 199, https://doi.org/10.1038/s41597-022-01332-3, 2022.

Levavasseur, G., Vrac, M., Roche, D. M., and Paillard, D.: Statistical Modelling of a New Global Potential Vegetation Distribution, Environ. Res. Lett., 7, 044 019, https://doi.org/10.1088/1748-9326/7/4/044019, 2012.

Lindgren, A., Lu, Z., Zhang, Q., and Hugelius, G.: Reconstructing Past Global Vegetation with Random Forest Machine Learning, Sacrificing the Dynamic Response for Robust Results, J. Adv. Model. Earth Syst., 13, e2020MS002 200, https://doi.org/10.1029/2020MS002200, 2021.

Loughran, T. F., Boysen, L., Bastos, A., Hartung, K., Havermann, F., Li, H., Nabel, J. E. M. S., Obermeier, W. A., and Pongratz, J.: Past and Future Climate Variability Uncertainties in the Global Carbon Budget Using the MPI Grand Ensemble, Glob. Biogeochem. Cycles, 35, e2021GB007 019, https://doi.org/10.1029/2021GB007019, 2021.

Luo, X., Zhou, H., Satriawan, T. W., Tian, J., Zhao, R., Keenan, T. F., Griffith, D. M., Sitch, S., Smith, N. G., and Still, C. J.: Mapping the Global Distribution of C4 Vegetation Using Observations and Optimality Theory, Nat. Commun., 15, 1219, https://doi.org/10.1038/s41467-024-45606-3, 2024.

Lyons, M. B., Keith, D. A., Phinn, S. R., Mason, T. J., and Elith, J.: A Comparison of Resampling Methods for Remote Sensing Classification and Accuracy Assessment, Remote Sens. Environ., 208, 145–153, https://doi.org/10.1016/j.rse.2018.02.026, 2018.

Marinova, E., Harrison, S. P., Bragg, F., Connor, S., de Laet, V., Leroy, S. A., Mudie, P., Atanassova, J., Bozilova, E., Caner, H., Cordova, C., Djamali, M., Filipova–Marinova, M., Gerasimenko, N., Jahns, S., Kouli, K., Kotthoff, U., Kvavadze, E., Lazarova, M., Novenko, E., Ramezani, E., Röpke, A., Shumilovskikh, L., Tanţău, I., and Tonkov, S.: Pollen–Derived Biomes in the Eastern Mediterranean–Black Sea–Caspian–Corridor, J. Biogeogr., 45, 484–499, https://doi.org/10.1111/jbi.13128, 2018.

Meyer, H. and Pebesma, E.: Predicting into Unknown Space? Estimating the Area of Applicability of Spatial Prediction Models, Methods Ecol. Evol., 12, 1620–1633, https://doi.org/10.1111/2041-210X.13650, 2021.

https://doi.org/10.5194/egusphere-2026-2682
Preprint. Discussion started: 3 June 2026

Meyer, H., Reudenbach, C., Wöllauer, S., and Nauss, T.: Importance of Spatial Predictor Variable Selection in Machine Learning Applications – Moving from Data Reproduction to Spatial Prediction, Ecol. Model., 411, 108 815, https://doi.org/10.1016/j.ecolmodel.2019.108815, 2019.

Moncrieff, G. R., Bond, W. J., and Higgins, S. I.: Revising the Biome Concept for Understanding and Predicting Global Change Impacts, J. Biogeogr., 43, 863–873, https://doi.org/10.1111/jbi.12701, 2016.

Obermeier, W. A., Nabel, J. E. M. S., Loughran, T., Hartung, K., Bastos, A., Havermann, F., Anthoni, P., Arneth, A., Goll, D. S., Lienert, S., Lombardozzi, D., Luyssaert, S., McGuire, P. C., Melton, J. R., Poulter, B., Sitch, S., Sullivan, M. O., Tian, H., Walker, A. P., Wiltshire, A. J., Zaehle, S., and Pongratz, J.: Modelled Land Use and Land Cover Change Emissions – a Spatio-Temporal Comparison of Different Approaches, Earth Syst. Dyn., 12, 635–670, https://doi.org/10.5194/esd-12-635-2021, 2021.

Obermeier, W. A., Schwingshackl, C., Ganzenmüller, R., Grassi, G., Heinrich, V., Luijkx, I. T., Bastos, A., Ciais, P., Sitch, S., and Pongratz, J.: Differences and Uncertainties in Land-Use CO2 Flux Estimates, Nat. Rev. Earth Environ., 6, 747–766, https://doi.org/10.1038/s43017-025-00730-6, 2025.

Olson, D. M., Dinerstein, E., Wikramanayake, E. D., Burgess, N. D., Powell, G. V. N., Underwood, E. C., D'amico, J. A., Itoua, I., Strand, H. E., Morrison, J. C., Loucks, C. J., Allnutt, T. F., Ricketts, T. H., Kura, Y., Lamoreux, J. F., Wettengel, W. W., Hedao, P., and Kassem, K. R.: Terrestrial Ecoregions of the World: A New Map of Life on Earth, BioScience, 51, 933–938, https://doi.org/10.1641/0006-3568(2001)051[0933:TEOTWA]2.0.CO;2, 2001.

Pedregosa, F., Varoquaux, G., Gramfort, A., Michel, V., Thirion, B., Grisel, O., Blondel, M., Prettenhofer, P., Weiss, R., Dubourg, V., Vanderplas, J., Passos, A., Cournapeau, D., Brucher, M., Perrot, M., and Duchesnay, É.: Scikit-Learn: Machine Learning in Python, J. Mach. Learn. Res., 12, 2825–2830, 2011.

Pongratz, J., Reick, C., Raddatz, T., and Claussen, M.: A Reconstruction of Global Agricultural Areas and Land Cover for the Last Millennium, Glob. Biogeochem. Cycles, 22, 1–16, https://doi.org/10.1029/2007GB003153, 2008.

Pongratz, J., Reick, C. H., Raddatz, T., and Claussen, M.: Effects of Anthropogenic Land Cover Change on the Carbon Cycle of the Last Millennium, Glob. Biogeochem. Cycles, 23, https://doi.org/10.1029/2009GB003488, 2009.

Pongratz, J., Reick, C. H., Houghton, R. A., and House, J. I.: Terminology as a Key Uncertainty in Net Land Use and Land Cover Change Carbon Flux Estimates, Earth Syst. Dyn., 5, 177–195, https://doi.org/10.5194/esd-5-177-2014, 2014.

Pongratz, J., Schwingshackl, C., Bultan, S., Obermeier, W., Havermann, F., and Guo, S.: Land Use Effects on Climate: Current State, Recent Progress, and Emerging Topics, Curr. Clim. Change Rep., 7, 99–120, https://doi.org/10.1007/s40641-021-00178-y, 2021.

Poulter, B., MacBean, N., Hartley, A., Khlystova, I., Arino, O., Betts, R., Bontemps, S., Boettcher, M., Brockmann, C., Defourny, P., Hagemann, S., Herold, M., Kirches, G., Lamarche, C., Lederer, D., Ottlé, C., Peters, M., and Peylin, P.: Plant Functional Type Classification for Earth System Models: Results from the European Space Agency's Land Cover Climate Change Initiative, Geosci. Model Dev., 8, 2315–2328, https://doi.org/10.5194/gmd-8-2315-2015, 2015.

Prentice, I. C., Guiot, J., Huntley, B., Jolly, D., and Cheddadi, R.: Reconstructing Biomes from Palaeoecological Data: A General Method and Its Application to European Pollen Data at 0 and 6 Ka, Clim. Dyn., 12, 185–194, https://doi.org/10.1007/s003820050102, 1996.

Qin, F., Zhao, Y., and Cao, X.: Biome Reconstruction on the Tibetan Plateau since the Last Glacial Maximum Using a Machine Learning Method, Sci. China Earth Sci., 65, 518–535, https://doi.org/10.1007/s11430-021-9867-1, 2022.

Qin, Z., Zhu, Y., Canadell, J. G., Chen, M., Li, T., Mishra, U., and Yuan, W.: Global Spatially Explicit Carbon Emissions from Land-Use Change over the Past Six Decades (1961–2020), One Earth, 7, 835–847, https://doi.org/10.1016/j.oneear.2024.04.002, 2024.

https://doi.org/10.5194/egusphere-2026-2682
Preprint. Discussion started: 3 June 2026

Ramankutty, N. and Foley, J. A.: Estimating Historical Changes in Global Land Cover: Croplands from 1700 to 1992, Glob. Biogeochem. Cycles, 13, 997–1027, https://doi.org/10.1029/1999GB900046, 1999.

Reick, C. H., Raddatz, T., Brovkin, V., and Gayler, V.: Representation of Natural and Anthropogenic Land Cover Change in MPI–ESM, J. Adv. Model. Earth Syst., 5, 459–482, https://doi.org/10.1002/jame.20022, 2013.

Roberts, D. R., Bahn, V., Ciuti, S., Boyce, M. S., Elith, J., Guillera–Arroita, G., Hauenstein, S., Lahoz–Monfort, J. J., Schröder, B., Thuiller, W., Warton, D. I., Wintle, B. A., Hartig, F., and Dormann, C. F.: Cross–Validation Strategies for Data with Temporal, Spatial, Hierarchical, or Phylogenetic Structure, Ecography, 40, 913–929, https://doi.org/10.1111/ecog.02881, 2017.

Rodriguez-Galiano, V. F., Ghimire, B., Rogan, J., Chica-Olmo, M., and Rigol-Sanchez, J. P.: An Assessment of the Effectiveness of a Random Forest Classifier for Land-Cover Classification, ISPRS J. Photogramm. Remote Sens., 67, 93–104, https://doi.org/10.1016/j.isprsjprs.2011.11.002, 2012.

Sankaran, M., Ratnam, J., and Hanan, N. P.: Tree–Grass Coexistence in Savannas Revisited – Insights from an Examination of Assumptions and Mechanisms Invoked in Existing Models, Ecol. Lett., 7, 480–490, https://doi.org/10.1111/j.1461-0248.2004.00596.x, 2004.

Schratz, P., Muenchow, J., Iturritxa, E., Richter, J., and Brenning, A.: Hyperparameter Tuning and Performance Assessment of Statistical and Machine-Learning Algorithms Using Spatial Data, Ecol. Model., 406, 109–120, https://doi.org/10.1016/j.ecolmodel.2019.06.002, 2019.

Schulze, K., Malek, Ž., and Verburg, P. H.: Towards Better Mapping of Forest Management Patterns: A Global Allocation Approach, For. Ecol. Manag., 432, 776–785, https://doi.org/10.1016/j.foreco.2018.10.001, 2019.

Sidumo, B., Sonono, E., and Takaidza, I.: An Approach to Multi-Class Imbalanced Problem in Ecology Using Machine Learning, Ecol. Inform., 71, 101 822, https://doi.org/10.1016/j.ecoinf.2022.101822, 2022.

Sitch, S., O'Sullivan, M., Robertson, E., Friedlingstein, P., Albergel, C., Anthoni, P., Arneth, A., Arora, V. K., Bastos, A., Bastrikov, V., Bellouin, N., Canadell, J. G., Chini, L., Ciais, P., Falk, S., Harris, I., Hurtt, G., Ito, A., Jain, A. K., Jones, M. W., Joos, F., Kato, E., Kennedy, D., Klein Goldewijk, K., Kluzek, E., Knauer, J., Lawrence, P. J., Lombardozzi, D., Melton, J. R., Nabel, J. E. M. S., Pan, N., Peylin, P., Pongratz, J., Poulter, B., Rosan, T. M., Sun, Q., Tian, H., Walker, A. P., Weber, U., Yuan, W., Yue, X., and Zaehle, S.: Trends and Drivers of Terrestrial Sources and Sinks of Carbon Dioxide: An Overview of the TRENDY Project, Glob. Biogeochem. Cycles, 38, e2024GB008 102, https://doi.org/10.1029/2024GB008102, 2024.

Smith, B., Wårlind, D., Arneth, A., Hickler, T., Leadley, P., Siltberg, J., and Zaehle, S.: Implications of Incorporating N Cycling and N Limitations on Primary Production in an Individual-Based Dynamic Vegetation Model, Biogeosciences, 11, 2027–2054, https://doi.org/10.5194/bg-11-2027-2014, 2014.

Smith, S. M., Geden, O., Gidden, M. J., Lamb, W. F., Nemet, G. F., Minx, J. C., Buck, H., Burke, J., Cox, E., Edwards, M. R., Johnstone, I., Müller-Hansen, F., Pongratz, J., Roe, S., Schenuit, F., and Vaughan, N. E., eds.: The State of Carbon Dioxide Removal 2024 - 2nd Edition, University of Oxford, https://doi.org/10.17605/OSF.IO/F85QJ, 2024.

Sobol, M. K. and Finkelstein, S. A.: Predictive Pollen-Based Biome Modeling Using Machine Learning, PLOS ONE, 13, e0202 214, https://doi.org/10.1371/journal.pone.0202214, 2018.

Stocker, B. D., Strassmann, K., and Joos, F.: Sensitivity of Holocene Atmospheric CO 2 and the Modern Carbon Budget to Early Human Land Use: Analyses with a Process-Based Model, Biogeosciences, 8, 69–88, https://doi.org/10.5194/bg-8-69-2011, 2011.

Sun, A., Luo, Y., Wu, H., Chen, X., Li, Q., Yu, Y., Sun, X., and Guo, Z.: An Updated Biomization Scheme and Vegetation Reconstruction Based on a Synthesis of Modern and Mid-Holocene Pollen Data in China, Glob. Planet. Change, 192, 103 178, https://doi.org/10.1016/j.gloplacha.2020.103178, 2020.

https://doi.org/10.5194/egusphere-2026-2682
Preprint. Discussion started: 3 June 2026

Svenning, J.-C. and Sandel, B.: Disequilibrium Vegetation Dynamics under Future Climate Change, Am. J. Bot., 100, 1266–1286, https://doi.org/10.3732/ajb.1200469, 2013.

Tucker, C., Brandt, M., Hiernaux, P., Kariryaa, A., Rasmussen, K., Small, J., Igel, C., Reiner, F., Melocik, K., Meyer, J., Sinno, S., Romero, E., Glennie, E., Fitts, Y., Morin, A., Pinzon, J., McClain, D., Morin, P., Porter, C., Loeffler, S., Kergoat, L., Issoufou, B.-A., Savadogo, P., Wigneron, J.-P., Poulter, B., Ciais, P., Kaufmann, R., Myneni, R., Saatchi, S., and Fensholt, R.: Sub-Continental-Scale Carbon Stocks of Individual Trees in African Drylands, Nature, 615, 80–86, https://doi.org/10.1038/s41586-022-05653-6, 2023.

Tüxen, R.: Die Heutige Potentielle Natürliche Vegetation Als Gegenstand Der Vegetationskartierung (Mit 3 Abb. Und 10 Tabellen), Angew. Pflanzensoziol. Stolzenau, 13, 4–42, 1956.

U.S. EPA: NA_CEC_Eco_Level1. Ecological Regions of North America Level I. 2010 Update, U.S. Environmental Protection Agency [data set], 2010.

Veloso, H. P., Oliveira Filho, L. C., Fonseca Vaz, A. M. S., Lima, M. P. M., Marquete, R., and Braza, J. E. M.: MANUAL Técnico Da Vegetação Brasileira, vol. n. 1 of *Série Manuais Técnicos Em Geociências*, IBGE, Rio de Janeiro, ISBN 85-240-0427-4, 1992.

Whittaker, R. H.: Communities and Ecosystems, Macmillan, New York, 2d ed. edn., ISBN 0-02-427390-2, 1975.

Winkler, K., Fuchs, R., Rounsevell, M., and Herold, M.: Global Land Use Changes Are Four Times Greater than Previously Estimated, Nat. Commun., 12, 2501, https://doi.org/10.1038/s41467-021-22702-2, 2021.

Wulder, M. A., Coops, N. C., Roy, D. P., White, J. C., and Hermosilla, T.: Land Cover 2.0, Int. J. Remote Sens., 39, 4254–4284, https://doi.org/10.1080/01431161.2018.1452075, 2018.

Wullschleger, S. D., Epstein, H. E., Box, E. O., Euskirchen, E. S., Goswami, S., Iversen, C. M., Kattge, J., Norby, R. J., van Bodegom, P. M., and Xu, X.: Plant Functional Types in Earth System Models: Past Experiences and Future Directions for Application of Dynamic Vegetation Models in High-Latitude Ecosystems, Ann. Bot., 114, 1–16, https://doi.org/10.1093/aob/mcu077, 2014.

Yang, J. and Huang, X.: The 30 m Annual Land Cover Dataset and Its Dynamics in China from 1990 to 2019, Earth Syst. Sci. Data, 13, 3907–3925, https://doi.org/10.5194/essd-13-3907-2021, 2021.

Yu, Z., Ciais, P., Piao, S., Houghton, R. A., Lu, C., Tian, H., Agathokleous, E., Kattel, G. R., Sitch, S., Goll, D., Yue, X., Walker, A., Friedlingstein, P., Jain, A. K., Liu, S., and Zhou, G.: Forest Expansion Dominates China's Land Carbon Sink since 1980, Nat. Commun., 13, 5374, https://doi.org/10.1038/s41467-022-32961-2, 2022.

Zhang, Z., Wang, Z., Zhang, X., Liang, B., and Wang, J.: Comprehensive Assessment of Potential Forestation Land in China Considering Factors of Vegetation Resilience and Top Vegetation Succession, Ecol. Indic., 166, 112 476, https://doi.org/10.1016/j.ecolind.2024.112476, 2024.